

SUBSURFACE OBSERVATIONS RELATED TO INFILTRATION AT YUCCA MOUNTAIN

Prepared for

**U.S. Nuclear Regulatory Commission
Contract NRC-02-07-006**

Prepared by

S. Stothoff

**Center for Nuclear Waste Regulatory Analyses
San Antonio, Texas**

October 2009

CONTENTS

Section	Page
FIGURES	iv
TABLES	viii
ACKNOWLEDGMENTS	ix
1 INTRODUCTION.....	1-1
2 SITE INFORMATION	2-1
3 GEOCHEMICAL INFORMATION	3-1
3.1 Matrix and Perched-Water Geochemical Observations	3-1
3.2 Perched Water	3-11
3.3 Estimated Borehole Fluxes	3-12
4 SEEPS AND DAMP SPOTS	4-1
4.1 South Ramp Seepage Observations.....	4-1
4.2 Exploratory Studies Facility Damp Spots and Blowing Fracture	4-9
4.3 South Ramp Lithology and Topology	4-10
4.4 Alcove 1 Infiltration Test.....	4-12
4.5 Local Distributed Infiltration Hypothesis	4-15
4.6 Channel Infiltration Hypothesis.....	4-16
4.7 Downdip Diversion Hypothesis.....	4-18
4.8 Summary	4-22
5 THERMAL MODEL	5-1
5.1 Analytic Solution.....	5-1
5.2 Sensitivity to Model Inputs.....	5-2
5.3 Input Parameters at Boreholes.....	5-4
5.4 Temperature Profiles at Boreholes.....	5-5
5.5 Estimated Borehole Fluxes	5-10
6 CHEMICAL AND THERMAL ANOMALIES	6-1
6.1 Geochemical Anomalies.....	6-1
6.2 Temperature Anomalies	6-4
6.3 Summary	6-7
7 INFERENCES	7-1
7.1 Chloride-Based and Temperature-Based Flux Comparisons.....	7-1
7.2 Tiva Canyon Caprock.....	7-2
7.3 Lithophysal and Nonlithophysal Units.....	7-4
7.4 Summary	7-6
8 REFERENCES.....	8-1

Contents (continued)

Section	Page
APPENDIX A—BOREHOLE GEOCHEMISTRY FIGURES	
APPENDIX B—THERMAL PROFILE FIGURES	
APPENDIX C—THERMAL CONDUCTIVITY ESTIMATES	

FIGURES

Figure	Page
2-1 Central Block Lithologic Map for Yucca Mountain. The Lithologic Map Is a Recolored Digital Version of the Day, et al. (1988) Map.....	2-2
2-2 A, B, G, H, P, and WT Series Boreholes.....	2-3
2-3 Boreholes Near the Potential Repository With Unsaturated Zone Thermal or Geochemical Observations.....	2-4
2-4 Location Map for Yucca Mountain.....	2-6
2-5 Estimated Median Bulk Filled-Fracture Saturated Hydraulic Conductivity.....	2-7
3-1 Chlorine-36 Observations in Drifts and the Deepest Observed Bomb-Pulse Chlorine-36 Observation in Boreholes.....	3-2
3-2 Tritium Observations in Drifts and the Deepest Observed Bomb-Pulse Tritium Observation in Boreholes.....	3-6
3-3 Approximate Percolation Flux Using Chloride Samples From Drifts and Perched Water.....	3-9
3-4 Maximum Observed Saturation (θ) at the Transition Between the Tiva Canyon Welded and Paintbrush Tuff Nonwelded Units.....	3-14
3-5 Geochemical Observations for SD-9 and Associated Thermohydrologic Properties.....	3-15
3-6 Geochemical Observations for SD-7 and Associated Thermohydrologic Properties.....	3-21
3-7 Geochemical Observations for UZ #16 and Associated Thermohydrologic Properties.....	3-23
3-8 Geochemical Observations for SD-12 and Associated Thermohydrologic Properties.....	3-24
3-9 Geochemical Observations for NRG-7a and Associated Thermohydrologic Properties.....	3-25
4-1 Time History of Daily and Cumulative Site 1 Precipitation and Penman Evapotranspiration and Seepage Measurements.....	4-2
4-2 Full-Periphery Map Displaying Locations of Seeps and Damp Spots.....	4-3
4-3 Features in the South Ramp of the Exploratory Studies Facility. Seep Samples, Damp Features, and the Blowing Fracture Are Drawn Over the Drift.....	4-4
4-4 Mean Observed Concentration at Each Seep Location, Plotted by Station.....	4-6
4-5 Mean Observed Concentration at Each Seep Location, Plotted by Depth Below Ground Surface.....	4-7
4-6 Mean Observed Concentration of Selected Species at Each Seep Location Between Stations 75+62 and 76+00.5.....	4-8
4-7 Three Hypothesized Source Locations for the South Ramp Seepage Event.....	4-13
4-8 Section of As-Built Full-Periphery Map Between Exploratory Studies Facility Stations 76+00 and 76+40.....	4-20
5-1 Response of a Temperature Profile to Percolation Flux in a Single Homogenous Layer and to Thermal Conductivity in Two Homogenous Layers.....	5-3
5-2 Digitized Temperatures in Boreholes Aligned North to South.....	5-6
5-3 Digitized Temperatures in Boreholes Aligned East to West.....	5-8
5-4 Digitized Temperatures in Boreholes With Water-Filled Access Tubes.....	5-9

FIGURES (continued)

Figure	Page
5-5 Percolation Flux Estimates, Temperature, and Thermohydrologic Properties for SD-12.....	5-11
5-6 Percolation Flux Estimates, Temperature, and Thermohydrologic Properties for NRG-6.....	5-12
5-7 Percolation Flux Estimates, Temperature, and Thermohydrologic Properties for NRG-7a.....	5-13
5-8 Percolation Flux Estimates, Temperature, and Thermohydrologic Properties for G-2.....	5-14
5-9 Comparison of Estimated Percolation Fluxes	5-16
6-1 Location of Boreholes With Geochemical and Temperature Anomalies Near Yucca Mountain	6-2
6-2 Drillhole Wash Temperature Profiles	6-6
A-1 Location Map for Boreholes With Geochemical Data	A-1
A-2 Geochemical Observations for G-2 and Associated Thermohydrologic Properties	A-2
A-3 Geochemical Observations for N-55 and Associated Thermohydrologic Properties	A-3
A-4 Geochemical Observations for NRG-6 and Associated Thermohydrologic Properties	A-4
A-5 Geochemical Observations for NRG-7a and Associated Thermohydrologic Properties	A-5
A-6 Geochemical Observations for SD-6 and Associated Thermohydrologic Properties	A-6
A-7 Geochemical Observations for SD-7 and Associated Thermohydrologic Properties	A-7
A-8 Geochemical Observations for SD-9 and Associated Thermohydrologic Properties	A-8
A-9 Geochemical Observations for SD-12 and Associated Thermohydrologic Properties	A-9
A-10 Geochemical Observations for UZ-7a and Associated Thermohydrologic Properties	A-10
A-11 Geochemical Observations for UZ-14 and Associated Thermohydrologic Properties	A-11
A-12 Geochemical Observations for UZ #16 and Associated Thermohydrologic Properties	A-12
A-13 Geochemical Observations for WT #24 and Associated Thermohydrologic Properties	A-13
B-1 Location Map for Boreholes With Estimates of Percolation Flux Using Temperature Profiles.....	B-1
B-2 Percolation Flux Estimates, Temperature, and Thermohydrologic Properties for NRG-6.....	B-2
B-3 Percolation Flux Estimates, Temperature, and Thermohydrologic Properties for NRG-7a.....	B-3

FIGURES (continued)

Figure	Page
B-4 Percolation Flux Estimates, Temperature, and Thermohydrologic Properties for SD-12	B-4
B-5 Percolation Flux Estimates, Temperature, and Thermohydrologic Properties for UZ #4	B-5
B-6 Percolation Flux Estimates, Temperature, and Thermohydrologic Properties for UZ #5	B-6
B-7 Percolation Flux Estimates, Temperature, and Thermohydrologic Properties for UZ-7a	B-7
B-8 Percolation Flux Estimates, Temperature, and Thermohydrologic Properties for G-1	B-8
B-9 Percolation Flux Estimates, Temperature, and Thermohydrologic Properties for G-2	B-9
B-10 Percolation Flux Estimates, Temperature, and Thermohydrologic Properties for G-3	B-10
B-11 Percolation Flux Estimates, Temperature, and Thermohydrologic Properties for G-4	B-11
B-12 Percolation Flux Estimates, Temperature, and Thermohydrologic Properties for H-1	B-12
B-13 Percolation Flux Estimates, Temperature, and Thermohydrologic Properties for H-3	B-13
B-14 Percolation Flux Estimates, Temperature, and Thermohydrologic Properties for H-4	B-14
B-15 Percolation Flux Estimates, Temperature, and Thermohydrologic Properties for H-5	B-15
B-16 Percolation Flux Estimates, Temperature, and Thermohydrologic Properties for H-6	B-16
B-17 Percolation Flux Estimates, Temperature, and Thermohydrologic Properties for WT-1	B-17
B-18 Percolation Flux Estimates, Temperature, and Thermohydrologic Properties for WT-2	B-18
B-19 Percolation Flux Estimates, Temperature, and Thermohydrologic Properties for WT #3	B-19
B-20 Percolation Flux Estimates, Temperature, and Thermohydrologic Properties for WT #4	B-20
B-21 Percolation Flux Estimates, Temperature, and Thermohydrologic Properties for WT #6	B-21
B-22 Percolation Flux Estimates, Temperature, and Thermohydrologic Properties for WT-7	B-22
B-23 Percolation Flux Estimates, Temperature, and Thermohydrologic Properties for WT-10	B-23
B-24 Percolation Flux Estimates, Temperature, and Thermohydrologic Properties for WT-11	B-24
B-25 Percolation Flux Estimates, Temperature, and Thermohydrologic Properties for WT #12	B-25

FIGURES (continued)

Figure	Page
B-26 Percolation Flux Estimates, Temperature, and Thermohydrologic Properties for WT #14	B-26
B-27 Percolation Flux Estimates, Temperature, and Thermohydrologic Properties for WT #15	B-27
B-28 Percolation Flux Estimates, Temperature, and Thermohydrologic Properties for WT #16	B-28
B-29 Percolation Flux Estimates, Temperature, and Thermohydrologic Properties for WT #17	B-29
B-30 Percolation Flux Estimates, Temperature, and Thermohydrologic Properties for WT #18	B-30

TABLES

Table		Page
3-1	Summary of Chloride Observations for Boreholes With Deep Perched Water Samples.....	3-13
5-1	Estimated Mean Annual Infiltration and Heat Flux Using the One-Dimensional Analytic Solution.....	5-17
5-2	Borehole Percolation Fluxes Estimated Using Temperature Observations	5-18
6-1	Geochemical Anomalies Indicating Potential Lateral Flow.....	6-3
6-2	Temperature Anomalies Indicating Potential Lateral Flow	6-4
C-1	Estimated Thermal Conductivity for GFM2000 Units. The <i>In-Situ</i> Bulk K Is Used for Calculations in This Report.....	C-3

ACKNOWLEDGMENTS

This report was prepared to document work performed by the Center for Nuclear Waste Regulatory Analyses (CNWRA[®]) for the U.S. Nuclear Regulatory Commission (NRC) under Contract No. NRC-02-07-006. The activities reported here were performed on behalf of the NRC Office of Nuclear Material Safety and Safeguards, Division of High-Level Waste Repository Safety. The paper is an independent product of CNWRA and does not necessarily reflect the views or regulatory position of NRC. The author would like to acknowledge the suggestions and comments made by J. Winterle and G. Wittmeyer, which improved the quality of the presentation. The author would like to thank L. Mulverhill for her editorial review and B. Street for her administrative support.

QUALITY OF DATA, ANALYSES, AND CODE DEVELOPMENT

DATA: All CNWRA-generated data contained in this report meet quality assurance requirements described in the Geosciences and Engineering Division Quality Assurance Manual. Sources of other data should be consulted for determining the level of quality of those data.

ANALYSES AND CODE: Microsoft[®] Excel[®] 2000 Version 9.0.3821 SR-1 (Microsoft Corporation, 2002) and MATLAB[®] Version 7.1.0.246 (The MathWorks, Inc., 2005) were used to generate results for this report and are considered uncontrolled software in accordance with the CNWRA software Technical Operating Procedure TOP-018, Development and Control of Scientific and Engineering Software.

References:

Microsoft Corporation. "Excel." Redland, Washington: Microsoft Corporation. 2002.

The MathWorks, Inc. "MATLAB." Version 7.1.0.246. Natick, Massachusetts: The MathWorks, Inc. 2005.

1 INTRODUCTION

Observations from the unsaturated zone of the subsurface at Yucca Mountain provide information regarding percolation fluxes, and by implication, net infiltration fluxes. Sandia National Laboratories (2007a); Bodvarsson, et al. (2003); Constantz, et al. (2003); and Sass, et al. (1988) have used temperature measurements to estimate percolation fluxes at Yucca Mountain. Sandia National Laboratories (2007a); CRWMS M&O (2003); Zhu, et al. (2003); and Guerin (2001), among others, have used geochemical observations (including chloride, chlorine-36, and tritium concentrations) to infer or constrain percolation fluxes at Yucca Mountain. This report is intended to present publicly available data in a compact format to aid in comparing and contrasting implications of the data. This report indicates some of the strengths and limitations of the approaches and relates observations at depth to specific features at the overlying ground surface. Comparing the set of subsurface observations to the overlying source of percolating waters provides insights into features at the ground surface that may influence infiltration. Such insights and comparisons provide additional constraints and confirmatory information for the Infiltration Tabulator for Yucca Mountain (ITYM)¹ model (Stothoff, 2008a). This report is the fourth report in a recent series of climate and infiltration reports, preceded by a literature review on climate and infiltration (Stothoff and Musgrove, 2006), a report estimating million-year-average infiltration at Yucca Mountain (Stothoff and Walter, 2007), and a report describing the ITYM model bases and confirmatory analyses (Stothoff, 2008a).

Inferences regarding infiltration fluxes can be drawn by assessing the influence of percolating water on temperatures within the subsurface. This is because water moving within a temperature gradient (such as the geothermal gradient) absorbs heat from and releases heat to the porous medium while advecting the absorbed energy, thereby altering the temperature gradient. The difference between measured temperature and temperatures calculated assuming pure conduction is measurable with sufficient water fluxes acting over sufficient distance. The heat balance method has the advantage that temperatures at a location in the unsaturated zone are strongly affected by conduction and thus represent a volumetric average of water fluxes much larger than the scale of the borehole. The representative scale represented by a temperature measurement is not well established, but it may be comparable to the 30-m [98-m] grid scale used for ITYM simulations. Percolation fluxes inferred using the heat balance method are sensitive to the uncertainty in thermal properties that are used in the analysis to describe the host rock.

Geochemical observations can also be used to estimate fluxes, such as inferences drawn from chloride concentrations and bomb-pulse chlorine-36 at depth. Geochemical methods use chemical and radioactive species in the water as tracers and are applied in hydrologic studies worldwide. Some methods use mass balance calculations to infer changes in water flux from changes in chemical concentrations, such as increased concentrations occurring because of evaporation. In some cases, the presence of a tracer such as a bomb-pulse radionuclide can constrain travel times, thereby providing information on water velocity and water flux. Geochemical data can be strongly affected by the path taken by the sampled water, and in the fractured rock at Yucca Mountain, where water takes tortuous paths through a heterogeneous subsurface, a given volume of porous medium typically intersects flowpaths with different travel times and origins. Geochemical data in the unsaturated zone are representative of an individual flowpath, and this flowpath is typically at a much finer scale than the scale represented by

¹Infiltration Tabulator for Yucca Mountain is used frequently throughout this report; therefore, the acronym ITYM will be used.

temperature perturbations. Geochemical observations often differ by a factor of two or more among samples separated by 1 to 2 m [3.3 to 6.6 ft] in Yucca Mountain, as shown in Section 3, implying that the scale for representativeness of geochemical data can be on the order of 1 m [3.3 ft] or less.

Chloride is a conservative natural tracer that remains in the liquid phase with minimal interaction with the porous medium; because of these properties, interpretations of chloride concentrations are more direct than most other tracers and the chloride-mass-balance method has been widely used in hydrologic investigations around the world. Chlorine-36 and tritium are naturally occurring isotopes of chlorine and hydrogen, respectively, that are also used as tracers indicating fast travel times through the subsurface. Elevated concentrations of chlorine-36, tritium, and other radioactive species were introduced to the environment worldwide by atomic bomb testing during the 1950s. Both the chlorine-36 to chloride concentration ratio and the tritium concentration can indicate whether the waters have a modern or bomb-pulse component (similar inferences can be drawn from other atomic testing byproducts), and inferences from the chlorine-36/chloride ratio and tritium concentration are commonly drawn in hydrologic investigations worldwide. The two isotopic tracers differ in that chlorine does not partition to the vapor phase, whereas tritium (because hydrogen is a component of water) readily partitions into the vapor phase.

This report summarizes geochemical and thermal information that the U.S. Department of Energy has been used to estimate net infiltration and deep percolation fluxes at Yucca Mountain. Background site information is presented in Section 2. Geochemical observations are described in Section 3. Hydrological observations related to the South Ramp seepage event and damp spots in the Exploratory Studies Facility, and geochemical observations related to the event, are described in Section 4. An analytic thermal model and comparisons with observations are described in Section 5. Section 6 describes geochemical and thermal observations indicative of lateral flow in the unsaturated zone. Section 7 contains inferences regarding infiltration and percolation for individual boreholes, the Exploratory Studies Facility, and the Enhanced Characterization of the Repository Block cross drift.

2 SITE INFORMATION

The interplay between surficial lithology, soil depth, and topography plays a strong role in determining infiltration patterns (Stothoff, 2008a). The current conceptual understanding of infiltration processes suggests that net infiltration exiting the evapotranspiration zone is greater in areas with shallow soil and a significant fracture volume fraction at the surface, and is less in areas with deep soil and few fractures. Net infiltration exiting the evapotranspiration zone may also occur in areas with significant soil depth when lateral flow provides additional waters for infiltration, such as in certain active channels and at the foot of some hillslopes. However, these locations are spatially limited and are thought to provide only a small fraction of the total mean annual infiltration (MAI)¹ at Yucca Mountain.

Lithology strongly influences fracture patterns at the top of the bedrock. Figure 2-1 reproduces the Day, et al. (1998) surficial geologic map, recolored to emphasize the hydrologic role of particular units. Three primary formations are indicated in the figure: the Tiva Canyon welded (TCw),² the Paintbrush Tuff nonwelded (PTn),³ and the Topopah Spring welded (TSw)⁴ formations. The TCw formation comprises zones from Tcrv through Tcu in Figure 2-1, the PTn comprises zones from Tbt5 through Ttrv, and the TSw (which is analogous to the TCw and only exposed on the west flank of Yucca Mountain) comprises zones from Ttrn3 through TtpII. Minor exposures of the Tiva Canyon tuffs (Tmr through Tpkt) are found, but not within the repository footprint. Deep alluvial and colluvial deposits are indicated by QTac and QTc in Figure 2-1. The Exploratory Studies Facility (ESF)⁵ and the Enhanced Characterization of the Repository Block (ECRB)⁶ are also color-coded by formation, with TCw, PTn, and TSw indicated by purple, yellow, and brown, respectively. Note that the same color codes are used to indicate geologic zones throughout this document.

TCw forms the topmost bedrock formation within most of the area of the unsaturated zone flow and transport model Sandia National Laboratories (2007a) considered; within the potential repository footprint, TCw is almost exclusively the topmost formation. For the purposes of estimating net infiltration, Stothoff (2008a) separates most of the TCw zones into three categories: moderately welded caprock (Tcrn4 through Tcr1 in Figure 2-1), lithophysal zones (Tcpul and TcplI), and nonlithophysal zones (Tcpun, Tcpmn, Tcpln, and Tcplnc). The Tcpum zone is described as grading from a lithophysal zone to a nonlithophysal zone, replacing the Tcplul and Tcplmn zones in the Day, et al. (1998) map. Stothoff (2008a) describes the caprock as having relatively high infiltration potential because of relatively large, weathered cooling joints separating massive rock blocks, even though the rock itself is relatively unfractured. Fractures in lithophysal zones tend to have larger apertures than in nonlithophysal zones, based on the detailed line survey in the ESF and ECRB (Stothoff, 2008a), but nonlithophysal zones tend to form fine-scale fracture networks. Caprock is indicated by shades of cyan, and nonlithophysal zones are redder than lithophysal zones in Figure 2-1.

Figures 2-2 and 2-3 identify the boreholes discussed in this report (the boreholes are indicated but not identified in Figure 2-1). Only the A, B, G, H, P, and WT series of boreholes are

¹Mean annual infiltration is used frequently throughout this report; therefore, the acronym MAI will be used.

²Tiva Canyon welded is used frequently throughout this report; therefore, the acronym TCw will be used.

³Paintbrush Tuff nonwelded is used frequently throughout this report; therefore, the acronym PTn will be used.

⁴Topopah Spring welded is used frequently throughout this report; therefore, the acronym TSw will be used.

⁵Exploratory Studies Facility is used frequently throughout this report; therefore, the acronym ESF will be used.

⁶Enhanced Characterization of the Repository Block is used frequently throughout this report; therefore, the acronym ECRB will be used.

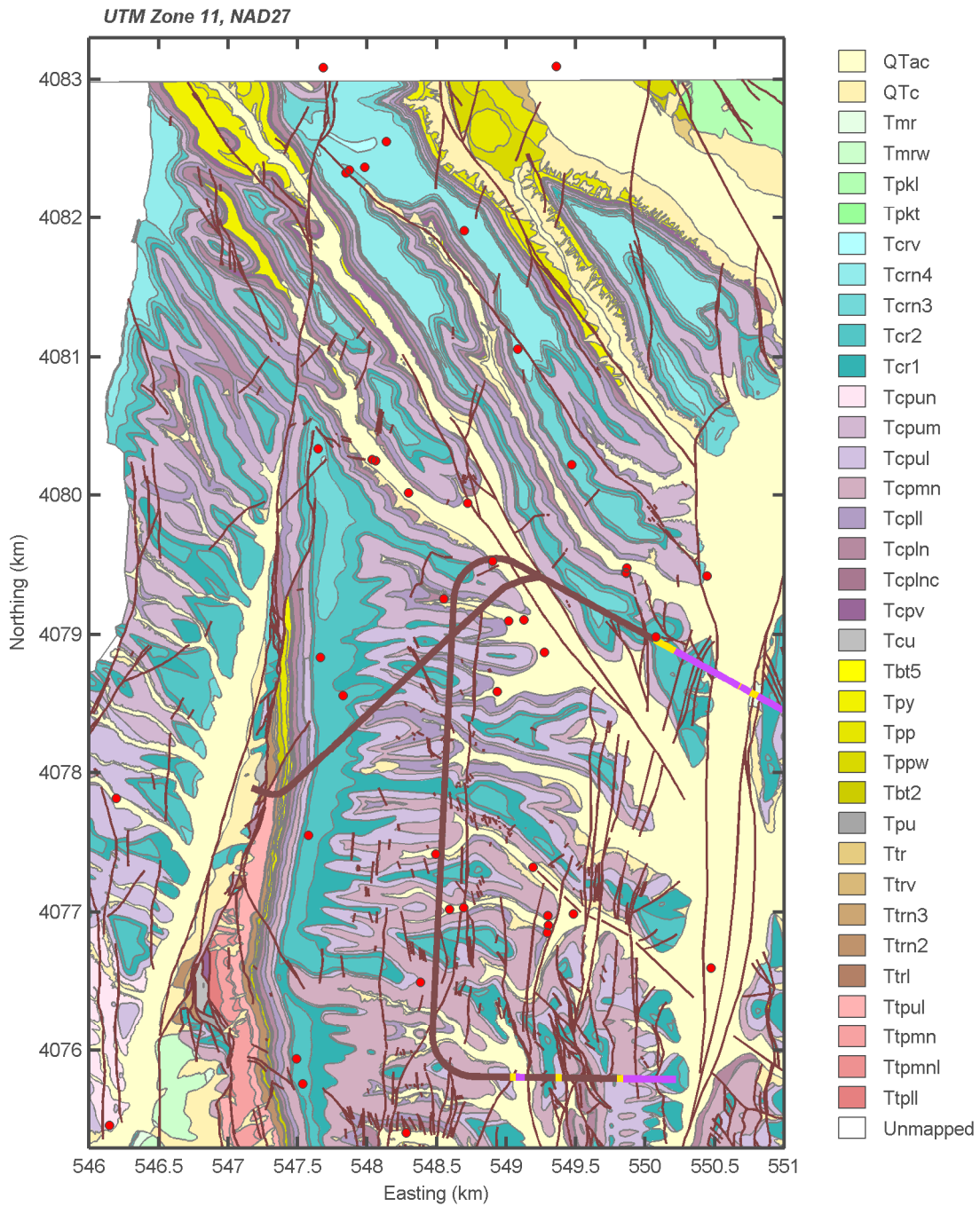


Figure 2-1. Central Block Lithologic Map for Yucca Mountain. The Lithologic Map Is a Recolored Digital Version of the Day, et al. (1998) Map. Boreholes Are Identified in Figure 2-3. [1 km = 0.62 mi]

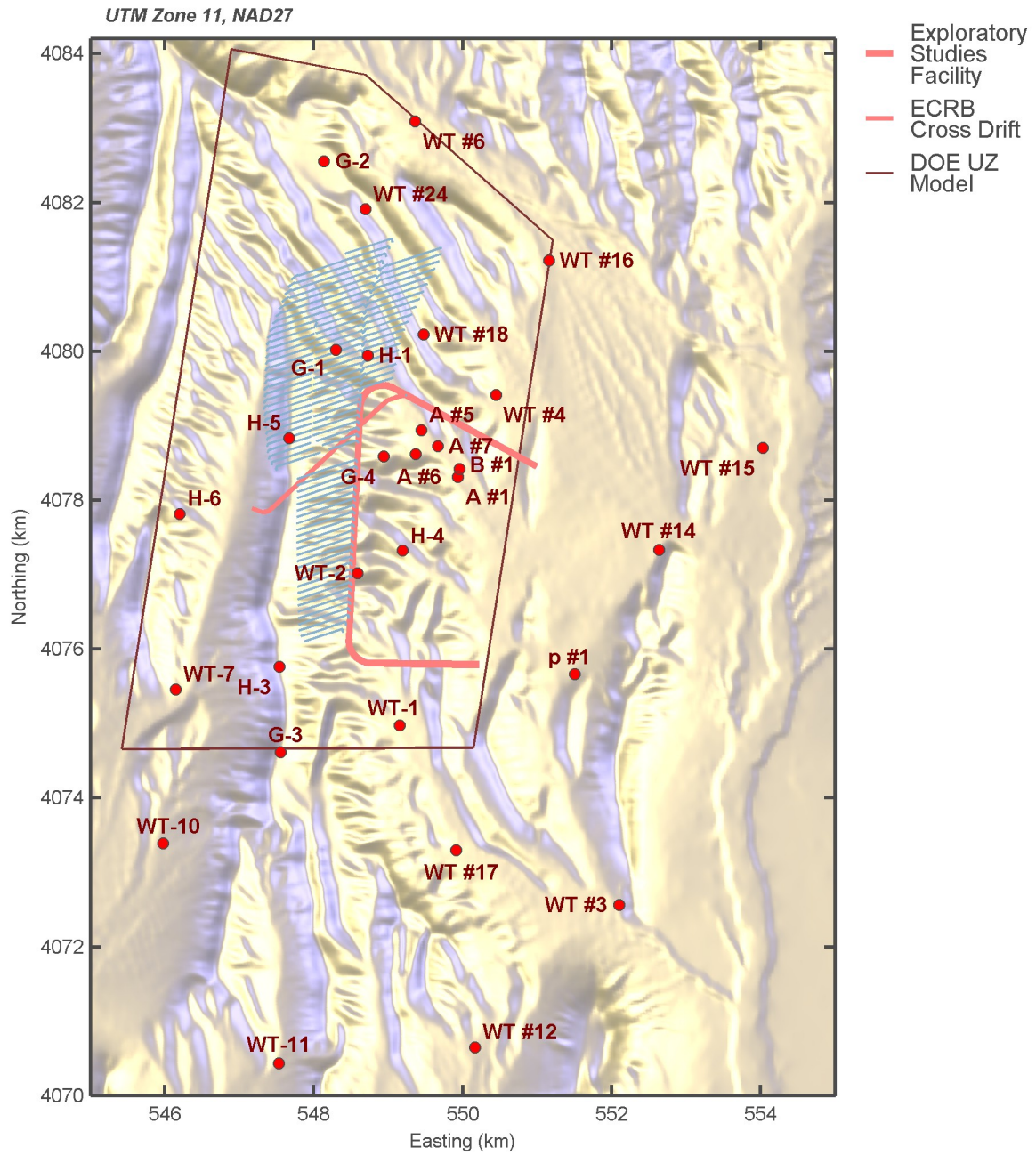


Figure 2-2. A, B, G, H, P, and WT Series Boreholes [1 km = 0.62 mi]

indicated in the larger scale Figure 2-2. The more immediate vicinity of the potential repository is shown in Figure 2-3; this figure also shows the Footprint Box Stothoff and Walter (2007) described and hatching indicating approximate drift locations for the potential repository [consistent with the repository block locations Sandia National Laboratories (2007a, Figure 6.1-1) described]. Figure 2-4 locates topographic features near Yucca Mountain. The background of the figures is derived from the seamless 10-m [32.8-ft] U.S. Geological Survey digital elevation model, available online (U.S. Geological Survey, 2006a). A morning lighting scheme is used, with south-facing shadows brightened with a blue light from the southwest.

Stothoff (2008a) combined the Day, et al. (1998) surficial geologic map with lithologic information to estimate the bulk filled-fracture K_{sat} indicated in Figure 2-5, where K_{sat} denotes saturated hydraulic conductivity. Stothoff (2008a) suggests that bulk filled-fracture saturated hydraulic conductivity may be one of the key lithologic factors controlling MAI. Red and blue tones in the figure indicate bulk filled-fracture K_{sat} ranges where the precise K_{sat} value is not significant for estimating MAI, based on inferences from infiltration modeling (Stothoff, 2008a). Red tones (the Tcrn3, Tcr2, and Tcr1 zones) indicate that bulk filled-fracture K_{sat} is inferred to be sufficiently large to not limit MAI, and blue tones (the PTn) indicate that K_{sat} is inferred to be so small that it essentially precludes MAI via the fracture system. Intermediate tones indicate a range over which the precise value for K_{sat} may be important in determining MAI values; densely welded zones typically are in this intermediate range. Field information is sparse regarding bulk filled-fracture saturated hydraulic conductivity; geochemical and geothermal information considered in later sections helps constrain MAI estimates in the TCw formation.

Analyses of subsurface geochemical and thermal observations may be useful in estimating MAI, but the characteristics of subsurface flow can complicate the analyses. Thermal analyses should be relatively unaffected by the heterogeneous nature of subsurface flow at small scales (e.g., partitioning of flow between matrix and fracture), because thermal transport is strongly diffusive. However, geochemical analyses are dependent on the details of the flow path, potentially including exchange between the matrix and fracture systems and different evaporative histories. Matrix–fracture interactions are thought to be minimal in densely welded zones (i.e., most of the TCw and TSw hydromechanical units) because the matrix K_{sat} is small. The PTn hydromechanical unit has a much more permeable matrix and has far fewer fractures than the welded units. This can potentially create a strong matrix–fracture exchange associated with the PTn as waters are imbibed from the TCw and PTn fracture systems into the PTn matrix near the top of the PTn and return to the TSw fracture system as a result of low-matrix-permeability TSw zones below the PTn. Matrix and fracture waters would tend to mix in areas where fracture waters enter the PTn matrix, reducing chemical disequilibrium between matrix and fracture waters as mixing occurs. If the imbibition process occurs from fractures and faults in the PTn, the potential for exchange increases with increasing PTn thickness. Moving from south to north across the site, the PTn thickness is 15, 28.7, 68.6, and 160.7 m [49, 94, 225, and 527 ft] in boreholes G-3, G-4, H-1, and G-2, respectively (Bechtel SAIC Company, LLC, 2004a). Accordingly, the PTn may be more effective at mixing matrix and fracture waters in the northern portion of the site.

Matrix–fracture interactions are particularly important in interpreting bomb-pulse radionuclides, such as chlorine-36 and tritium, because observations of bomb-pulse radionuclides at depth imply that these tracers have reached the observation point since the 1950s. Bomb-pulse chlorine-36 has been found through the TCw, into the PTn, and even into the TSw in samples from boreholes located in shallow soil, but it is generally retained in the top 2 to 3 m [7 to 10 ft] of soil where the soil is deep (CRWMS M&O, 2003). Bomb-pulse tritium has been found as

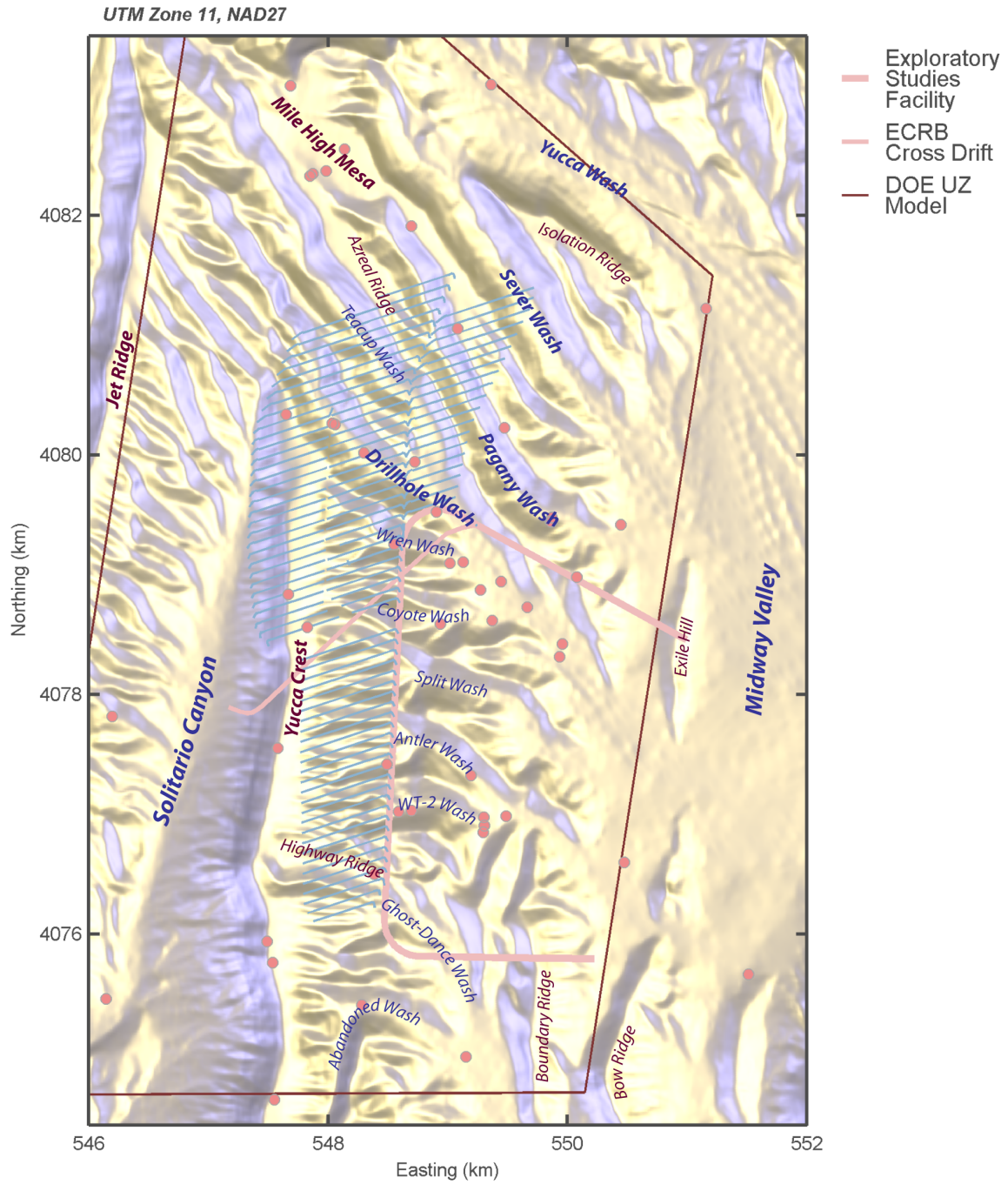


Figure 2-4. Location Map for Yucca Mountain [1 km = 0.62 mi]

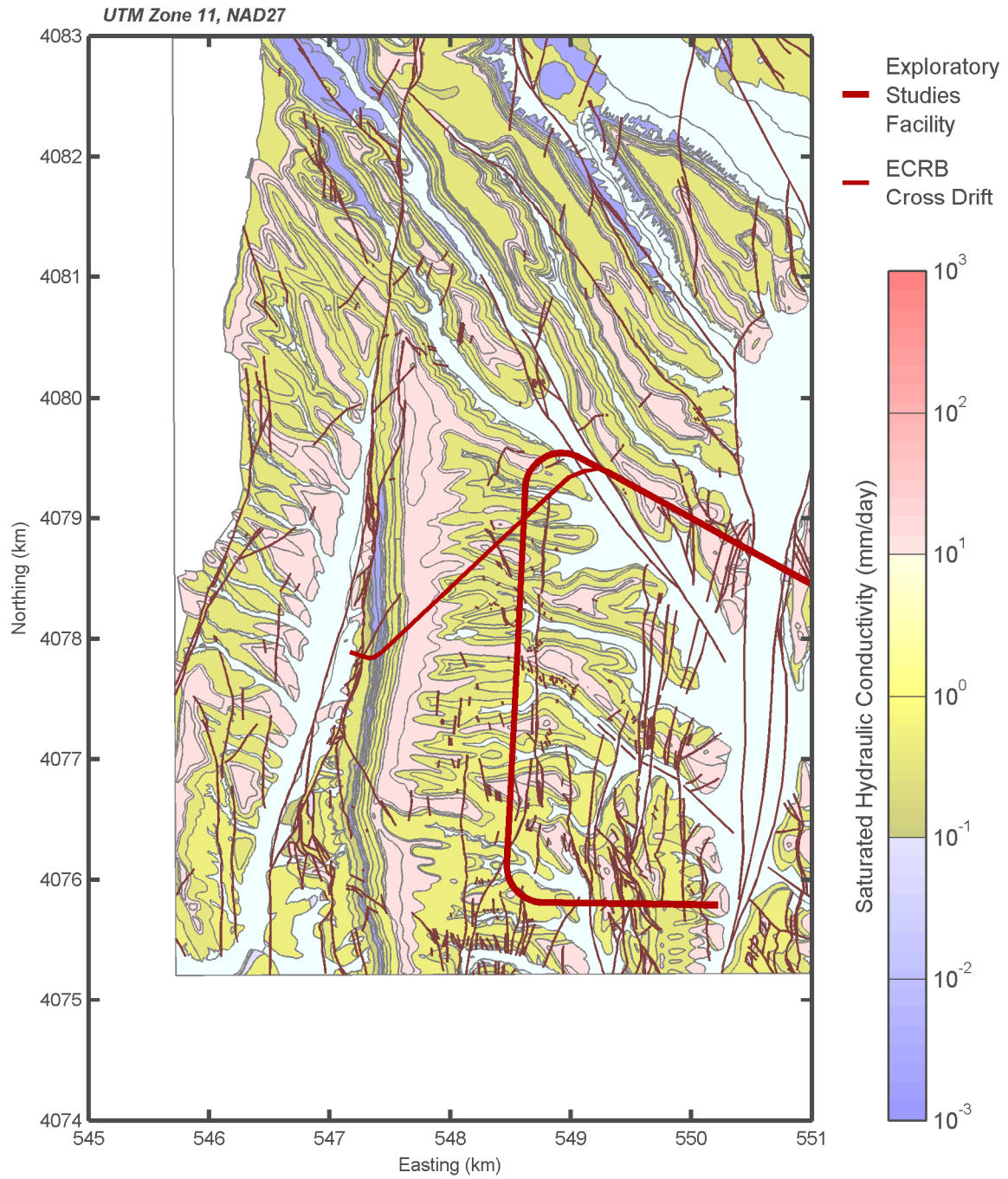


Figure 2-5. Estimated Median Bulk Filled-Fracture Saturated Hydraulic Conductivity
[Reproduced From Stothoff (2008a, Figure 6-15)]
[1 km = 0.62 mi; 25.4 mm/day = 1 in/day]

deep as the Calico Hills units below the potential repository horizon in four of the seven boreholes penetrating these units. Samples taken from the ESF and ECRB shortly after tunneling was completed contained concentrations of chlorine-36 inferred to represent bomb-pulse concentrations in certain locations; more recent studies have been unable to either reproduce or invalidate these observations (U.S. Geological Survey, 2006b). CRWMS M&O (2003) inferred that bomb-pulse chlorine-36 observed below the PTn unit requires both relatively large MAI and a breach in the PTn (such as occurs with a fault).

Chlorine-36 generally remains in the liquid phase as chloride, but tritium partitions between the liquid and vapor phases. An observation of bomb-pulse chlorine-36 in a sample implies that the sampled water entered the ground in the 1950s or later, because chlorine-36 is restricted to liquid pathways for transport. An observation of bomb-pulse tritium, however, does not necessarily imply that the sampled water entered during or after the 1950s because tritium disperses readily in the gas phase. Tritium may be transported from source waters in the gas phase by (i) bulk movement of the gas phase, (ii) net diffusion of vapor within the gas phase because of vapor-pressure gradients, and (iii) diffusion of tritium within vapor. Bulk movement of the gas phase may be the dominant transport mechanism above the PTn, because topographic, barometric, and wind-induced effects all are active above the PTn. Within and below the PTn, diffusion of tritium within vapor may be the dominant vapor-phase transport mechanism.

3 GEOCHEMICAL INFORMATION

3.1 Matrix and Perched-Water Geochemical Observations

Geochemical information at Yucca Mountain has been collected from matrix pore waters, perched water, the saturated zone, and seepage waters. Matrix pore-water samples were extracted from core samples obtained from boreholes and from the Exploratory Studies Facility (ESF),¹ Enhanced Characterization of the Repository Block (ECRB)² cross drift, and associated niches and alcoves; all references to pore waters herein refer to matrix waters as distinct from perched or fracture waters. Water samples were obtained from perched waters and the saturated zone by both bailing and pumping from boreholes. Perched water bodies penetrated by southern boreholes yielded relatively little water before going dry during pumping, whereas pumping from the northern perched water lasted longer, consistent with relatively local perched zones in the south and more extensive perching in the north. CRWMS M&O (2003) describes the sampling program for these sources in detail. Section 4 discusses seeps and damp features in the ESF, including geochemical observations related to seepage waters.

Chloride samples have been obtained for matrix pore waters from the ESF, ECRB, and boreholes. Chloride samples of perched and saturated zone waters have also been obtained. Almost all chlorine-36 samples are from the ESF and ECRB, with some samples obtained from boreholes. The borehole chlorine-36 samples are primarily of perched waters or saturated zone waters, and no perched or saturated zone waters within or near the three-dimensional unsaturated zone flow and transport model domain had waters with an inferred bomb-pulse chlorine-36 signature. Samples indicating bomb-pulse chlorine-36 were obtained from the shallow perched zone in UE-29 UZN #91 and the shallow saturated zone in boreholes UE-29 a #1 and UE-29 a #2, all located in upper Fortymile Wash more than 8 km [5 mi] northeast of the nearest corner of the model domain. Tritium samples were obtained from the ESF, ECRB Cross Drift, and boreholes. Early analyses used an analytical procedure that had an analytical standard deviation of 4 tritium units (TU)³ [CRWMS M&O (2003)], where 1 TU indicates 1 tritium atom in 10^{18} hydrogen atoms. Samples from the ESF and ECRB, aside from samples obtained from Alcove 2, were subsequently analyzed for lower levels of tritium using an enrichment process that produced an analytical standard deviation as low as 0.1 TU (Bechtel SAIC Company, LLC, 2004b, Section 6.14.2.2.1).

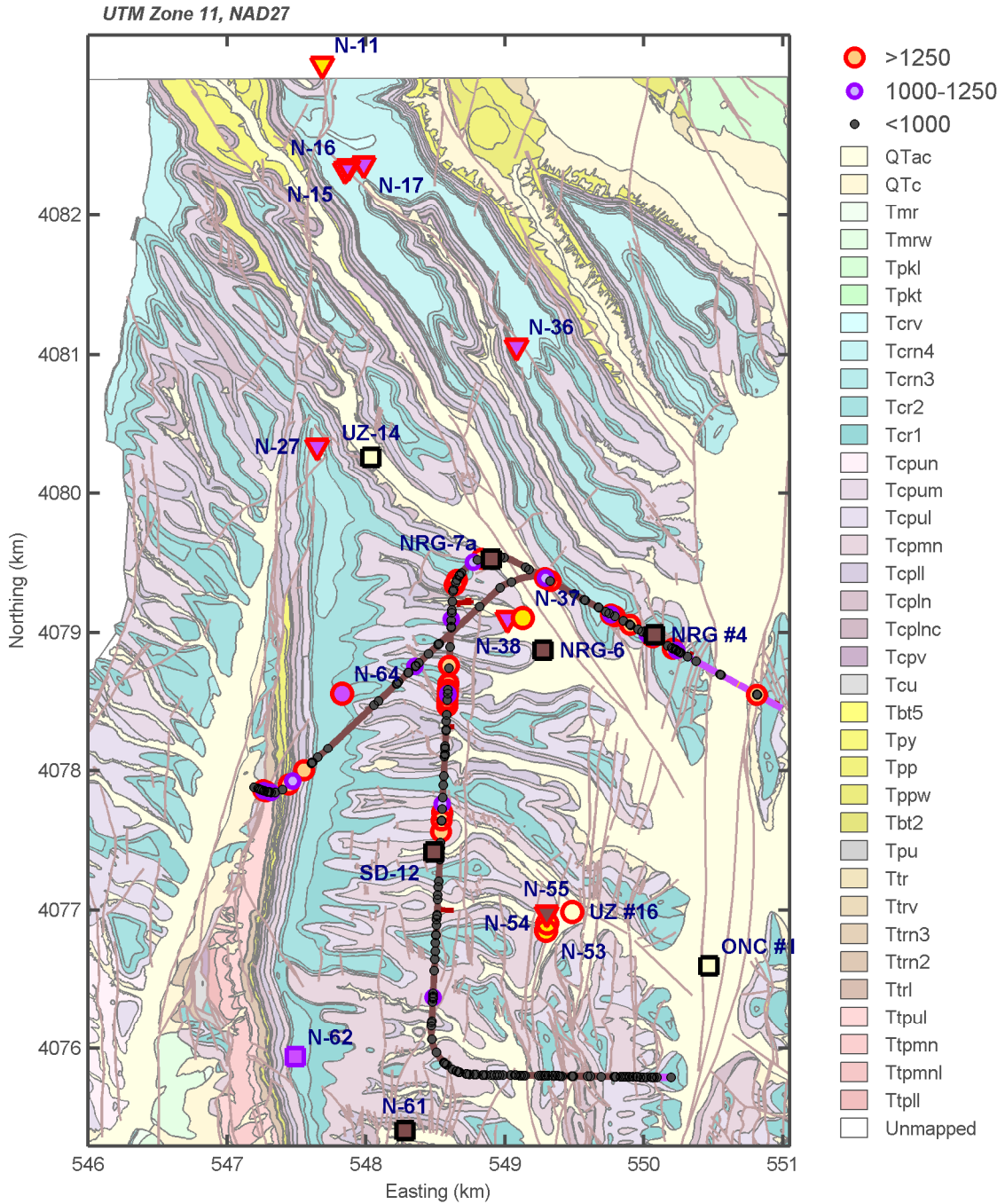
Matrix pore-water samples were primarily obtained from nonwelded units, because of the difficulty in obtaining water samples from low-porosity, low-permeability welded tuffs. The difficulty in obtaining water samples may result in chloride estimates that include rock chloride (CRWMS M&O, 2003). Such interactions would tend to yield chloride estimates that are overly concentrated in chloride, especially in welded units. Rock chloride is low in chlorine-36 because of its age, implying that bomb-pulse chlorine-36 pore-water estimates could be also masked by old chloride released as rock was crushed during sampling. CRWMS M&O (2003) notes that the sampling procedure used in the ESF is less prone to release of rock chloride than the sampling procedure using borehole cuttings.

The spatial distribution of chlorine-36 observations is summarized in Figure 3-1, including drift observations from the ESF and ECRB as well as information about the deepest

¹Exploratory Studies Facility is used frequently throughout this report; therefore, the acronym ESF will be used.

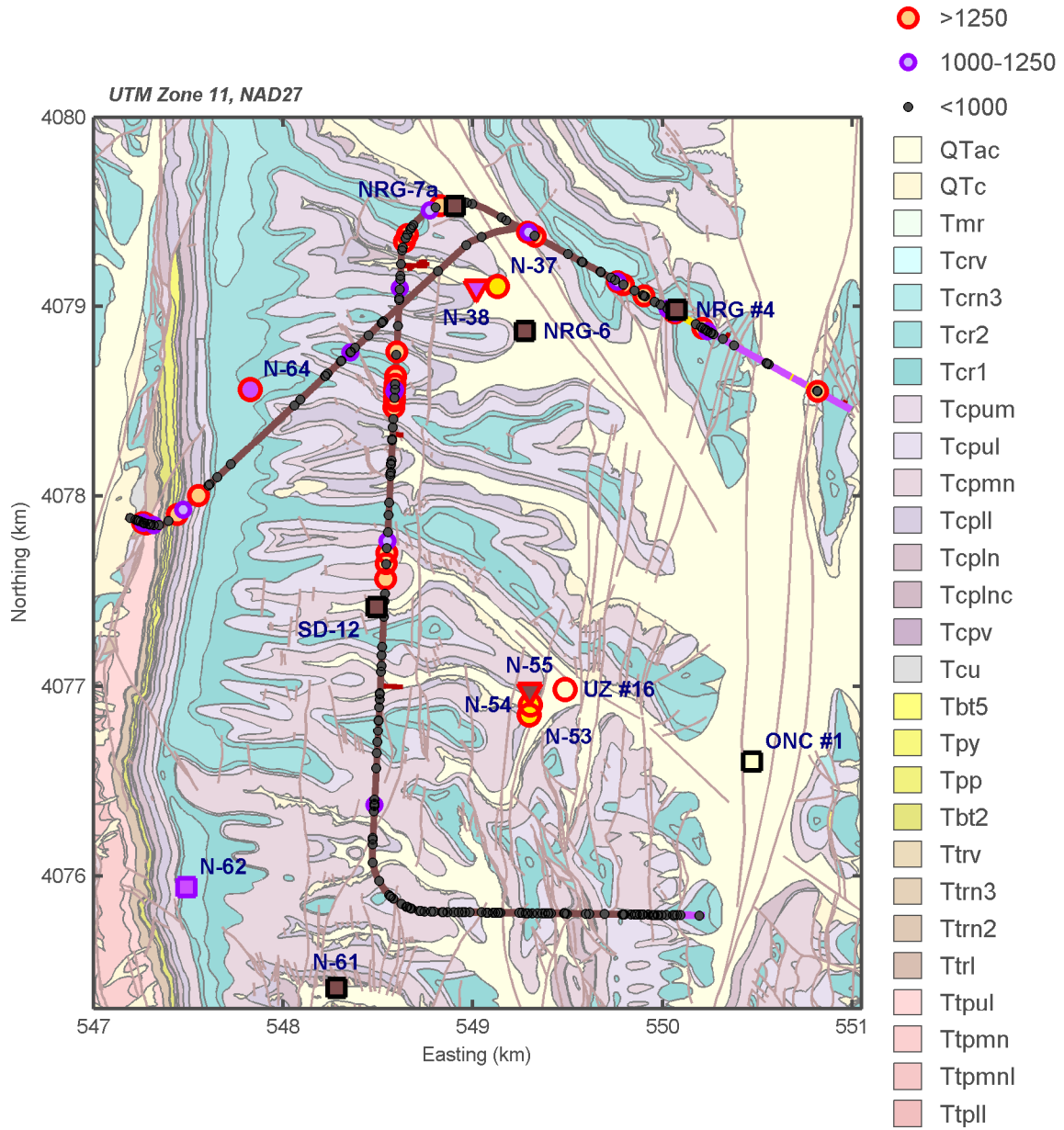
²Enhanced Characterization of the Repository Block is used frequently throughout this report; therefore, the acronym ECRB will be used.

³Tritium units is used frequently throughout this report; therefore, the acronym TU will be used.



(a)

Figure 3-1. Chlorine-36 Observations in Drifts and the Deepest Observed Bomb-Pulse Chlorine-36 Observation in Boreholes. (a) Observations Near the Potential Repository. [1 km = 0.62 mi; Chlorine-36 Reported in Units of Atoms Cl-36/Atoms Cl × 10¹⁵]



(b)
Figure 3-1 (continued). (b) Observations in and Near Drifts.
 [1 km = 0.62 mi; Chlorine-36 Reported in Units of Atoms Cl-36/Atoms Cl × 10¹⁵]

observed chlorine-36 sampled from boreholes. The ECRB observations are taken from the U.S. Geological Survey (2006b, Table 4-17); the ESF observations from the U.S. Geological Survey (2006b, Appendix A); and the borehole observations from Fabryka-Martin, et al. (1996, Tables 5-5 and B; 1997, Table 4-11).

Chlorine-36 is cosmogenically produced. The chlorine-36/chloride ratio in precipitation at present, and prior to the 1950s, is approximately 500×10^{-15} , but this ratio averaged 900×10^{-15} during the late Pleistocene and peaked at approximately $1,100 \times 10^{-15}$ during the Pleistocene (Fabryka-Martin, et al., 1996, Section 4.1.3). Peak atmospheric chlorine-36/chloride ratios greater than $200,000 \times 10^{-15}$ were observed in the late 1950s. Because chlorine-36 has a half-life of approximately 300,000 years, the chlorine-36/chloride ratio is relatively inert in groundwater. CRWMS M&O (2003, Section 6.6.3) describes chlorine-36 characteristics in greater detail, suggesting that groundwater chlorine-36/chloride ratios greater than $1,250 \times 10^{-15}$ show an unambiguous bomb-pulse signature. Fabryka-Martin, et al. (1996, Section 4.1.3) indicate that radioactive decay of chlorine-36 from the Pleistocene peak would provide a present-day ratio of approximately $1,000 \times 10^{-15}$. Murphy (1997) suggests that samples with a chlorine-36/chloride ratio greater than 900×10^{-15} to $1,000 \times 10^{-15}$ are likely to have a bomb pulse component based on statistical arguments.

Borehole observations shown in Figure 3-1 are indicated by red triangles if the deepest sample had a bomb-pulse signature (i.e., chlorine-36/chloride ratio greater than $1,250 \times 10^{-15}$), red circles if a bomb-pulse sample was underlain by a sample lacking the bomb-pulse signature, black squares if no bomb-pulse sample was identified, and purple squares if a sample with a ratio above the peak natural ratio was identified (i.e., chlorine-36/chloride ratio greater than $1,000 \times 10^{-15}$). The color of the fill identifies the hydromechanical unit with the deepest bomb-pulse signature or the shallowest sample if no bomb-pulse sample was obtained. Note that many of the samples were obtained from shallow neutron-probe boreholes.

Boreholes with chlorine-36 observations are located along ridgetops, at the base of sideslopes, or in alluvium. All ridgetop boreholes north of the ESF (N-11, N-15, N-16, N-17, N-27, and N-36) are neutron-probe boreholes and had bomb-pulse chlorine-36 at the lowest sampled location, typically within the Tiva Canyon formation, and all but one are within approximately 50 m [160 ft] of a mapped fault. Five of these boreholes have a depth between 18.3 and 25.7 m [60 and 84.4 ft]; N-27 is 61.7 m [202.4 ft] deep. All of the northern ridgetop boreholes had maximum chlorine-36/chloride ratios greater than 10^{-11} ; only one other borehole (neutron probe borehole N-55 in WT-2 Wash) had comparably elevated chlorine-36 observations. The two other boreholes on Yucca Crest (N-62 and N-64) are 18.3-m [60-ft]-deep neutron-probe boreholes terminating in the Tiva Canyon formation, but are less directly associated with a fault than the northern ridgetop boreholes and had a smaller chlorine-36 signature. The two boreholes in a large channel bottom (N-37 and N-54) both exhibit bomb-pulse signatures in the upper alluvium and Paintbrush Tuff nonwelded (PTn)⁴ unit, but have low values in the intervening Tiva Canyon welded (TCw)⁵ unit. Nearby sideslope boreholes (N-38, N-53, and N-55) have bomb-pulse signatures in the TCw and (for N-53 and N-55) in the PTn (N-38 terminates in the TCw).

⁴Paintbrush Tuff nonwelded is used frequently throughout this report; therefore, the acronym PTn will be used.

⁵Tiva Canyon welded is used frequently throughout this report; therefore, the acronym TCw will be used.

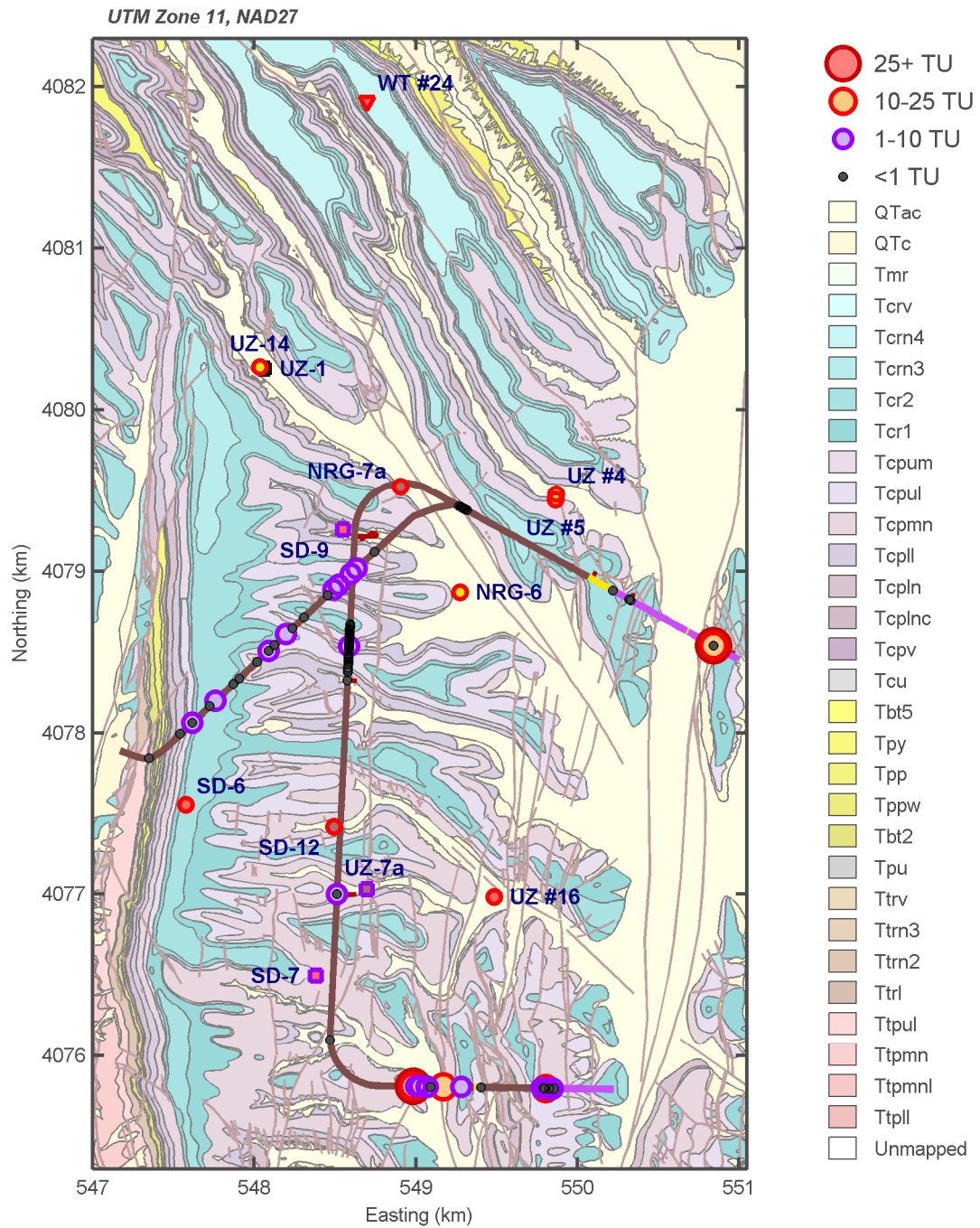
Only borehole N-55, a sideslope borehole, exhibited bomb-pulse chlorine-36 in the Topopah Spring welded (TSw)⁶ unit out of 10 boreholes with observations in the TSw. One ridgetop borehole (NRG-4) penetrates the TSw, with a single sample taken at a depth of 175 m [574 ft]. Four sideslope boreholes in addition to N-55 penetrate the TSw; the uppermost sample from boreholes NRG-6, NRG-7a, and SD-12 were obtained at a depth of at least 161.5 m [530 ft], and borehole N-61 lies in alluvium at the base of a south-facing slope. Two boreholes in alluvium had no bomb-pulse signature: ONC-1, with a minimum sample depth of 6.4 m [21 ft], and UZ-14, with a minimum sample depth of 1.8 m [6 ft]. Another borehole in alluvium (UZ-16) had a shallow bomb-pulse signature at the top of the profile. Large channel borehole N-37 does not exhibit a bomb-pulse signature in the TSw but does have a signature in the lowest sample obtained from the PTn.

Tritium is cosmogenically produced, like chlorine-36, yielding estimated midlatitude atmospheric concentrations of approximately 10 TU. Concentrations in precipitation prior to the 1950s were between 2 and 25 TU. Annual average atmospheric concentrations over 1,000 TU were observed in Albuquerque, New Mexico, and Salt Lake City, Utah, peaking in 1963. Because tritium has a half-life of 12.3 years, groundwater infiltrating with a concentration of 10 TU in 1952 would have a concentration of less than 1 TU when the tritium observations were made (i.e., starting in the 1990s). CRWMS M&O (2003, Section 6.6.2) describes tritium characteristics in greater detail, suggesting that groundwater tritium concentrations greater than 25 TU in the samples considered show an unambiguous bomb-pulse signature and noting that the analytical procedures used to estimate Yucca Mountain tritium concentrations had an analytical standard deviation of 4 TU. CRWMS M&O (2003, Section 6.6.2.1) notes that precipitation was low from 1958 through 1964 (years with the peak atmospheric tritium concentrations), concluding that the peak concentrations of tritium from those years may have been predominantly lost to evapotranspiration. Guerin (2001) further suggests that, accounting for analytical uncertainties, Yucca Mountain waters with tritium concentrations as low as 7 TU may indicate some component of bomb-pulse precipitation.

Bechtel SAIC Company, LLC (2004b, Section 6.14.2.2) describes low-level tritium analyses of cores obtained from horizontal boreholes in the ESF, ECRB, and associated alcoves. These analyses were not considered by CRWMS M&O (2003). Bechtel SAIC Company, LLC (2004b, Section 6.14.2.2) uses a criterion of 1 TU to indicate a sample with some component of a bomb-pulse signature, noting that contamination from construction water (with no measurable tritium) would reduce tritium concentrations and noting that prolonged contact with the atmosphere would change sample tritium concentrations to approximately 8 to 10 TU. Bechtel SAIC Company, LLC (2004b, Section 6.14.2.2) uses measured tritium minus twice the analytic standard deviation as an indication that the measured value is unambiguously above the criterion.

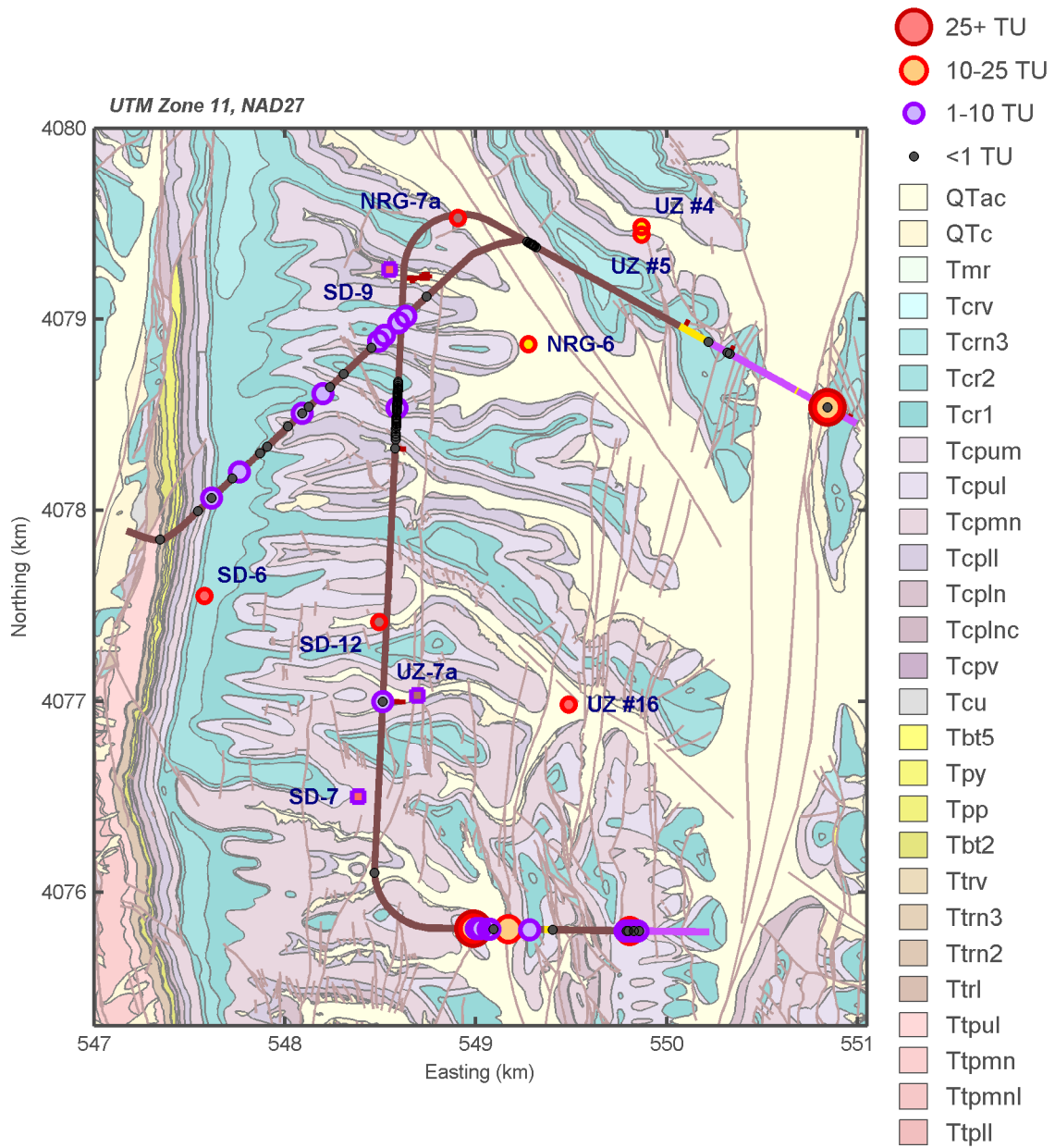
Figure 3-2 summarizes the spatial distribution of tritium observations, including low-level tritium observations from the ESF and ECRB as well as information about the deepest observed tritium sampled from surface boreholes. Observations from the ESF and ECRB are taken from Bechtel SAIC Company, LLC (2004b, Table 6-42) and observations from surface boreholes are taken from CRWMS M&O (2003, Tables 10 through 12). Borehole observations in Figure 3-2 use the same color scheme as boreholes in Figure 3-1, with a tritium concentration >25 TU considered

⁶Topopah Spring welded is used frequently throughout this report; therefore the acronym TSw will be used.



(a)

Figure 3-2. Tritium Observations in Drifts and the Deepest Observed Bomb-Pulse Tritium Observation Boreholes. (a) Observations Near the Potential Repository. [1 km = 0.62 mi; Tritium Reported in Tritium Units]



(b)
 Figure 3-2 (continued). (b) Observations in and Near Drifts.
 [1 km = 0.62 mi; Tritium Reported in Tritium Units]

an unambiguous bomb-pulse observation and a tritium concentration >7 TU considered an ambiguous bomb-pulse observation. The ESF and ECRB samples are coded to indicate samples above 1 TU, which indicate the potential for some bomb-pulse tritium, and to indicate samples above 10 TU, which indicate samples with tritium greater than present-day atmospheric concentrations.

Tritium levels indicative of unambiguous bomb-pulse conditions (i.e., greater than 25 TU) within and below the PTn have been observed in boreholes UZ #16, SD-12, SD-6, NRG-6, NRG-7a, UZ #4, UZ #5, and WT-24. Unambiguous bomb-pulse tritium samples were obtained below the TSw unit in boreholes SD-6, SD-12, UZ #16, and WT-24. Boreholes SD-7, SD-9, and UZ-14 do not have unambiguous bomb-pulse tritium observations but do have tritium observations at levels suggesting bomb-pulse tritium may form a component of the water (i.e., 7 to 25 TU) below the TSw unit. Unambiguous bomb-pulse tritium is generally missing from borehole samples from rock overlying the PTn, except for samples from UZ #5 collected prior to the existing U.S. Department of Energy quality assurance program. No deep perched water or aquifer sample within the three-dimensional unsaturated zone flow and transport model domain shows an unambiguous indication of bomb-pulse tritium, although a perched water sample from NRG-7a does suggest a partial indication at 10 TU.

Several low-level samples from the vicinity of the Bow Ridge Fault in Alcove 2 near the North Portal are above 25 TU (as large as 155 TU), and the sample in the South Ramp that is farthest from the South Portal is 25 TU. The elevated sample nearest the South Portal was obtained from the PTn unit, approximately 24 m from an exhaling fracture, and has a measured value of 12.5 TU. The tritium concentrations in this vicinity may be affected by interactions with the atmosphere.

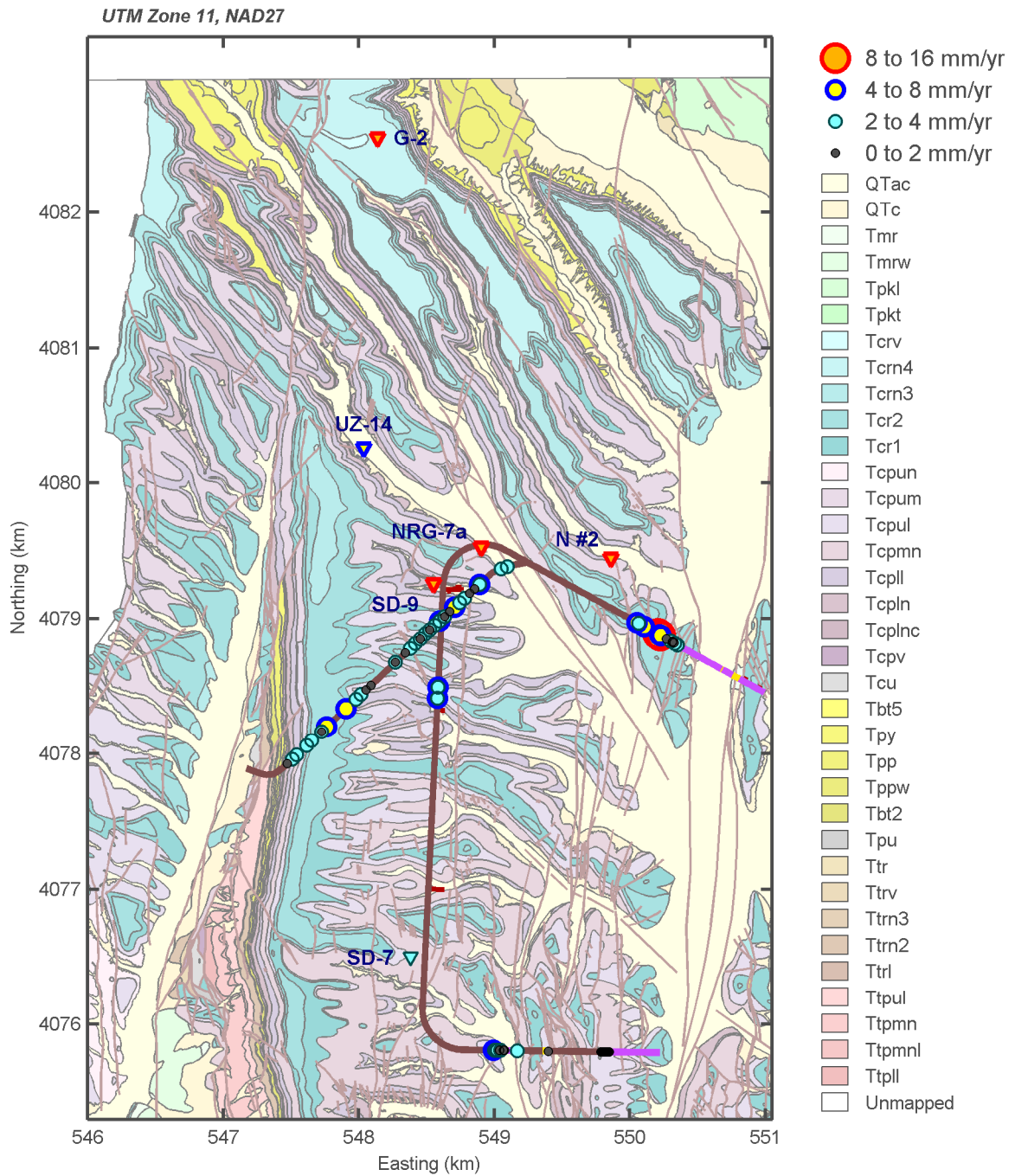
Chloride samples from the ESF, ECRB, deep perched water (G-2, NRG-7a, SD-7, SD-9, and UZ-14), and shallow ephemeral perched water (N #2) are shown in Figure 3-3. The chloride observations are presented in terms of estimated mean annual infiltration (MAI)⁷ using the chloride-mass-balance relationship describing a packet of liquid water unmixed with other waters (CRWMS M&O, 2003)

$$c_p P = c_w q_w \quad (3-1)$$

where c_p is effective chloride concentration for precipitation, c_w is the sampled chloride concentration at depth, P is mean annual precipitation, and q_w is mean annual volumetric water flux per unit area. Representative present-day values are used for Figure 3-3: $P = 185$ mm/yr [7.3 in/yr] (Stothoff, 2008a) and $c_p = 0.35$ mg/L [0.35 ppm] (CRWMS M&O, 2003).

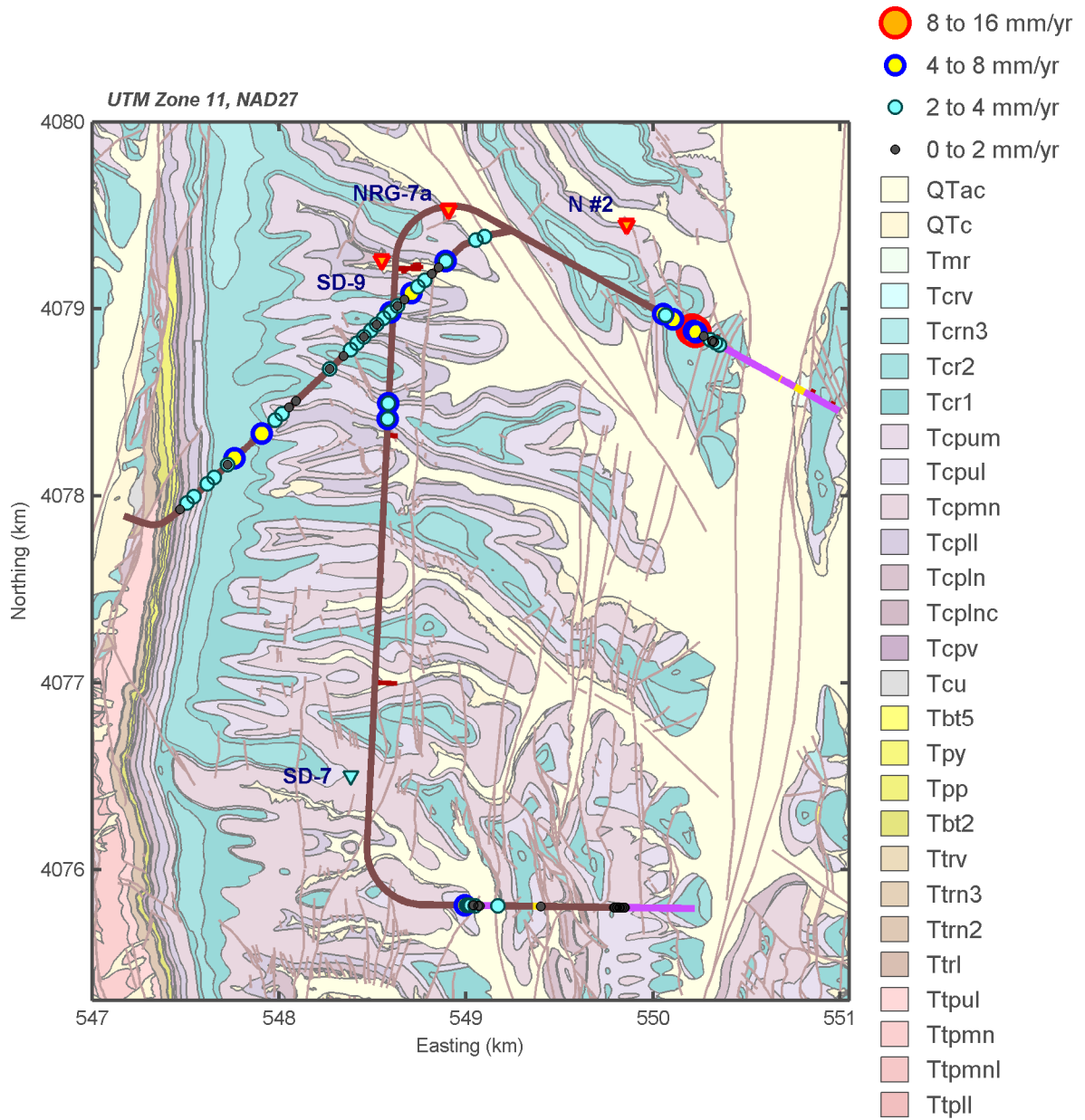
Except for two samples on the North Ramp of the ESF, all of the ESF and ECRB chloride samples have q_w less than 6 mm/yr [0.24 in/yr] using these parameters and the average q_w for these samples is 2.6 mm/yr [0.10 in/yr]. All of the dilute samples in the North Ramp have the Tcr2 zone of the Tiva Canyon caprock cropping out at the ground surface identified in the Infiltration Tabulator for Yucca Mountain (ITYM)⁷ model as a unit expected to have relatively

⁷Mean annual infiltration is used frequently throughout this report; therefore, the acronym MAI will be used.



(a)

Figure 3-3. Approximate Percolation Flux Using Chloride Samples From Drifts and Perched Water. Percolation Flux Is Estimated by $\{(185 \text{ mm/yr})[0.35 \text{ mg/L}]\}/C_w$, Where C_w Is the Sampled Chloride Concentration. (a) Observations Near the Potential Repository. [1 km = 0.62 mi; 25.4 mm/yr = 1 in/yr; 1 mg/L = 1 ppm]



(b)

Figure 3-3 (continued). (b) Observations in and Near Drifts
[1 km = 0.62 mi; 25.4 mm/yr = 1 in/yr]

large MAI. These dilute samples were obtained from the PTn exposed within the ESF. The most dilute of these samples were obtained near the TCw/PTn contact.

3.2 Perched Water

Deep perched water has been sampled in, from south to north, boreholes SD-7, SD-9, NRG-7a, UZ-14, and G-2. Deep perched water is found associated with low-permeability zones at the base of the TSw or with an altered zeolitic zone in the Calico Hills nonwelded (CHn)⁸ unit in these boreholes. Borehole SD-12 also exhibited a damp zone at the base of the TSw, as determined by a video camera log, but no seepage into the borehole was observed (CRWMS M&O, 2003, Section 6.5.2). Observed chloride concentrations for the deep perched waters and samples obtained from the matrix above and below the uppermost perched water observation are summarized in Table 3-1. Perched water samples from UZ-14 contained traces of drilling fluids from borehole G-1 (CRWMS M&O, 2003, Section 6.5.2), so the UZ-14 chemistry may be partially representative of G-1 drilling fluids. Also, Table 3-1 omits a UZ-14 perched water sample of 15.6 mg/L [15.6 ppm], approximately twice as concentrated as any other perched water sample from this borehole, because it was obtained shortly after a well development procedure that may have contaminated the sample.

In the four boreholes with samples from both the deep perched waters and the rock matrix, the perched water samples in Table 3-1 were more dilute than any matrix sample within the same borehole, and the average pore water concentration in the 100 m [330 ft] below the top of perching is between 4.3 and 8.7 times larger than the average perched water concentration. Only 1 of 121 borehole pore-water samples had a smaller chloride concentration than any perched sample. Average matrix chloride concentration within the 100 m [330 ft] below the top of the perched zone is lower than average matrix chloride concentration within the 100 m [330 ft] above the perched zone by a factor between 1.7 and 2.0 in two boreholes and is higher by a factor of 1.4 in another.

Transient shallow perched water was observed in Pagany Wash (neutron borehole N #2), associated with channel infiltration into alluvium above bedrock. The observed chloride concentration was 5.9 mg/L [5.9 ppm] for the perched water sample reported in DTN LAJF831222AQ98.011. CRWMS M&O (2003, Figure 10) compiles observed chloride concentration values that lie between 1 and 12 mg/L [1 and 12 ppm] for runoff in the Yucca Mountain area and 0.5 to 4 mg/L [0.5 to 4 ppm] for the higher elevation 3 Springs and East Stewart basins in the Kawich Range northwest of Yucca Mountain.

Low-permeability zones analogous to the TSw to CHn transition are found at the transition from the welded TCw to the nonwelded PTn for the boreholes shown in Figure 3-4. Damp zones, but not perched water, have been identified at all but one of these horizons in the ESF, as described in Section 4.2. Core samples from this transition zone in boreholes N-55, NRG-6, NRG-7a, SD-7, SD-9, SD-12, UZ-7a, UZ-14, and UZ-16 all demonstrate nearly saturated conditions where the matrix permeability transitions from values small relative to inferred infiltration rates (implying fracture-dominated flow) to values large relative to inferred infiltration rates (implying matrix-dominated flow). A nearly perched zone forming above a highly permeable zone would be expected if (i) the fracture system in the densely welded zone

⁸Calico Hills nonwelded is referenced frequently throughout this report; therefore, the acronym CHn will be used.

terminates in or above the moderately welded transition zone and (ii) the matrix permeability has values comparable to the infiltration pulses reaching that location. Water would transfer from the fracture system to the matrix at the rate that the matrix can accept water or at the rate of percolation flux, whichever is smaller. If the matrix permeability is locally too small to accept an infiltration pulse, lateral redistribution to a more permeable pathway would be promoted within the fracture system.

Using Eq. (3-1) to interpret chloride concentrations with representative present-day values for effective chloride concentration and precipitation, all of the perched waters have q_w between 7 and 15 mm/yr [0.28 and 0.59 in/yr]. The average perched-water value is 10 mm/yr [0.39 in/yr] within the unsaturated zone model domain; only the northernmost of these boreholes (G-2) lies within 200 m [660 ft] of an outcrop of a caprock unit. These values do not necessarily correspond to areal average infiltration either at present or in the past, because this would require that all transport pathways (e.g., matrix, fracture, and fault) are fully mixed at the sample location and the waters from each pathway are representative of the same climate.

Mass balance requirements suggest that waters with the chemistry observed during the South Ramp seepage event described in Section 4 cannot be the primary source of the perched water, because waters with a chloride concentration of 41 mg/L [41 ppm], the most dilute chloride concentration Oliver and Whelan (2006) and Cizdziel, et al. (2008) reported for the seepage event, must be diluted by more than a factor of 4 with rainwater to achieve the highest observed perched-water chloride concentration reported in Table 3-1.

3.3 Estimated Borehole Fluxes

Geochemical observations provide an indirect means for inferring percolation fluxes, and the context of a geochemical observation can be important for the inferences. Is an observation from the matrix or the fracture system? Is the observation potentially affected by lateral percolation? Is the observation potentially affected by the relative difficulty of sampling from welded units, or is it more easily obtained? Are there factors that may have altered the geochemical signature during travel from the initial infiltration location to the observation location? Is the observation representative of present-day climate, or is it possibly old enough to have experienced significantly different prior climatic conditions?

The plots in Section 3.3 and Appendix A display geochemical borehole observations with supplemental information that provides context for the geochemical data. The plots summarize a great deal of relevant information, including borehole location; surface characteristics affecting infiltration; nature of the geologic units; position of the observations relative to the potential repository horizon, water table, and perched water bodies; and the likely balance of matrix and fracture flow throughout the column. With this contextual information, the likely location of lateral flow and matrix–fracture interactions in the profile can be inferred and the geochemical data can be examined to see whether some facet of the data is consistent with such flow features.

Figure 3-5 illustrates how the supplemental information augments the geochemical observations in SD-9. The two inset windows in the leftmost panel (marked A in Figure 3-5) indicate that SD-9 is more or less in the center of the U.S. Department of Energy unsaturated zone site-scale model in one of the small washes east of Yucca Crest near the Little Prow; referring to

**Table 3-1. Summary of Chloride Observations for Boreholes
With Deep Perched Water Samples**

	Borehole				
	SD-7	SD-9	NRG-7a	UZ-14	G-2
Perched water samples					
Number	23	2	5	10	1
Minimum (mg/L)	4.0	5.6	7	6.13	6.5
Maximum (mg/L)	5.0	6.67	9.96	7.94	6.5
Mean (mg/L)	4.4	6.1	9.0	7.1	6.5
All pore-water samples above perching					
Number	5	31	12	22	0
Minimum (mg/L)	25.1	8.6	26	44	—
Maximum (mg/L)	133	337	53.6	245	—
Mean (mg/L)	58.9	88.5	37.6	93.1	—
Pore-water samples <100 m [330 ft] above perching					
Number	3	12	9	2	0
Minimum (mg/L)	25.1	8.6	26	88	—
Maximum (mg/L)	30.1	133	50	88	—
Mean (mg/L)	28.0	43.7	36.4	88	—
All pore-water samples below perching					
Number	9	9	0	33	0
Minimum (mg/L)	15	11	—	10	—
Maximum (mg/L)	83	50.2	—	130	—
Mean (mg/L)	35.6	25.7	—	33.7	—
Pore-water samples <100 m [330 ft] below perching					
Number	3	8	0	16	0
Minimum (mg/L)	18	11	—	10.6	—
Maximum (mg/L)	65	50.2	—	130	—
Mean (mg/L)	38.0	26.3	—	45.1	—
Ratio of minimum pore water to maximum perched					
All samples above	5.0	1.3	2.6	5.5	—
Samples <100 m [330 ft] above	5.0	1.3	2.6	5.5	—
All samples below	3.0	1.6	—	1.3	—
Samples <100 m [330 ft] below	3.6	1.6	—	1.3	—
Ratio of average pore water to average perched					
All samples above	13.5	14.4	4.2	13.1	—
Samples <100 m [330 ft] above	6.4	7.1	4.0	12.4	—
All samples below	8.1	4.2	—	4.8	—
Samples <100 m [330 ft] below	8.7	4.3	—	6.4	—
Ratio of average pore-water samples <100 m [330 ft] above perching to <100 m [330 ft] below	0.7	1.7	—	2.0	—

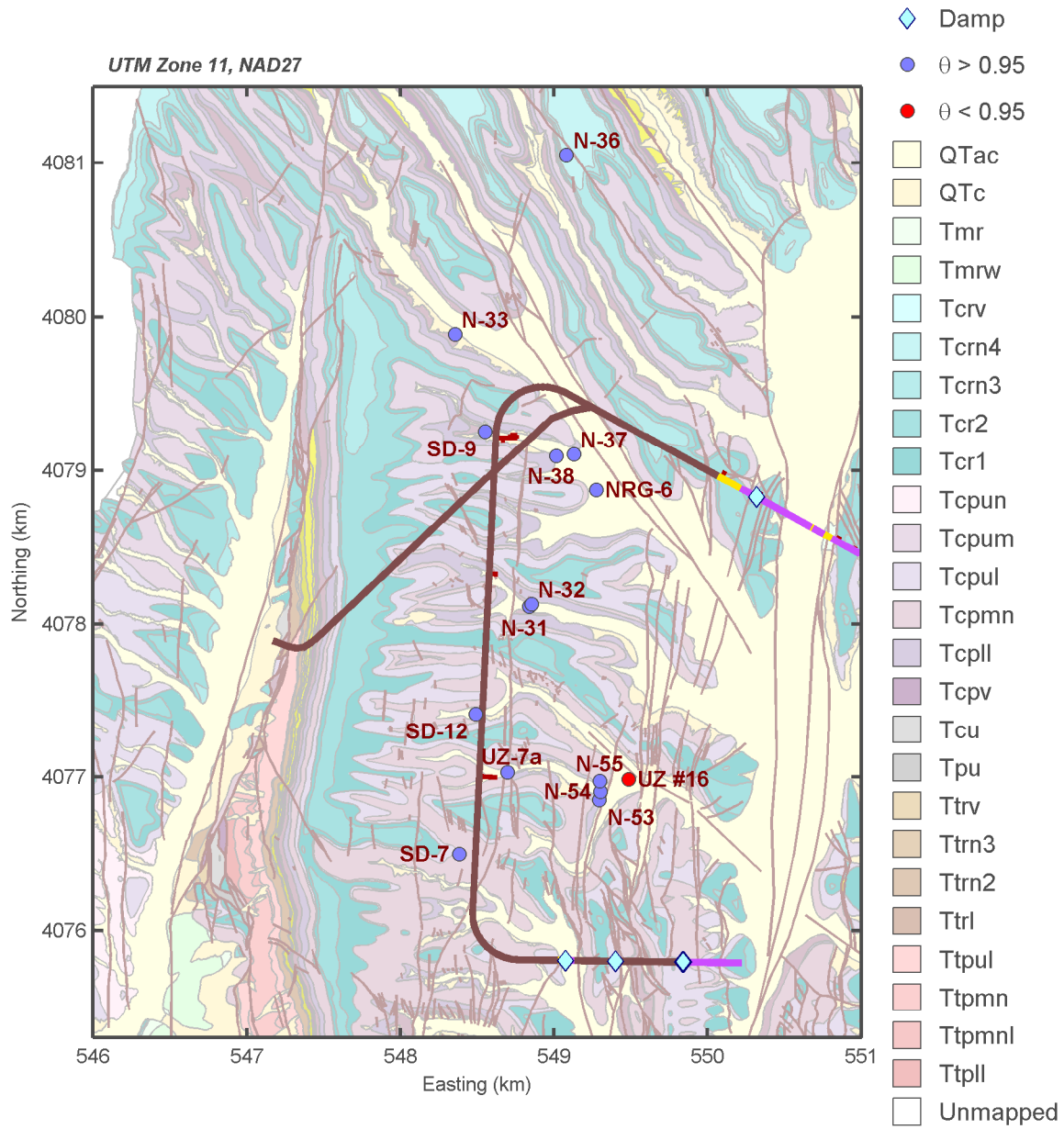


Figure 3-4. Maximum Observed Saturation (θ) at the Transition Between the Tiva Canyon Welded and Paintbrush Tuff Nonwelded Units. Observed Damp Spots in the Exploratory Studies Facility at the Same Transition Zone Are Indicated for Reference. [1.6 km = 1 mi]

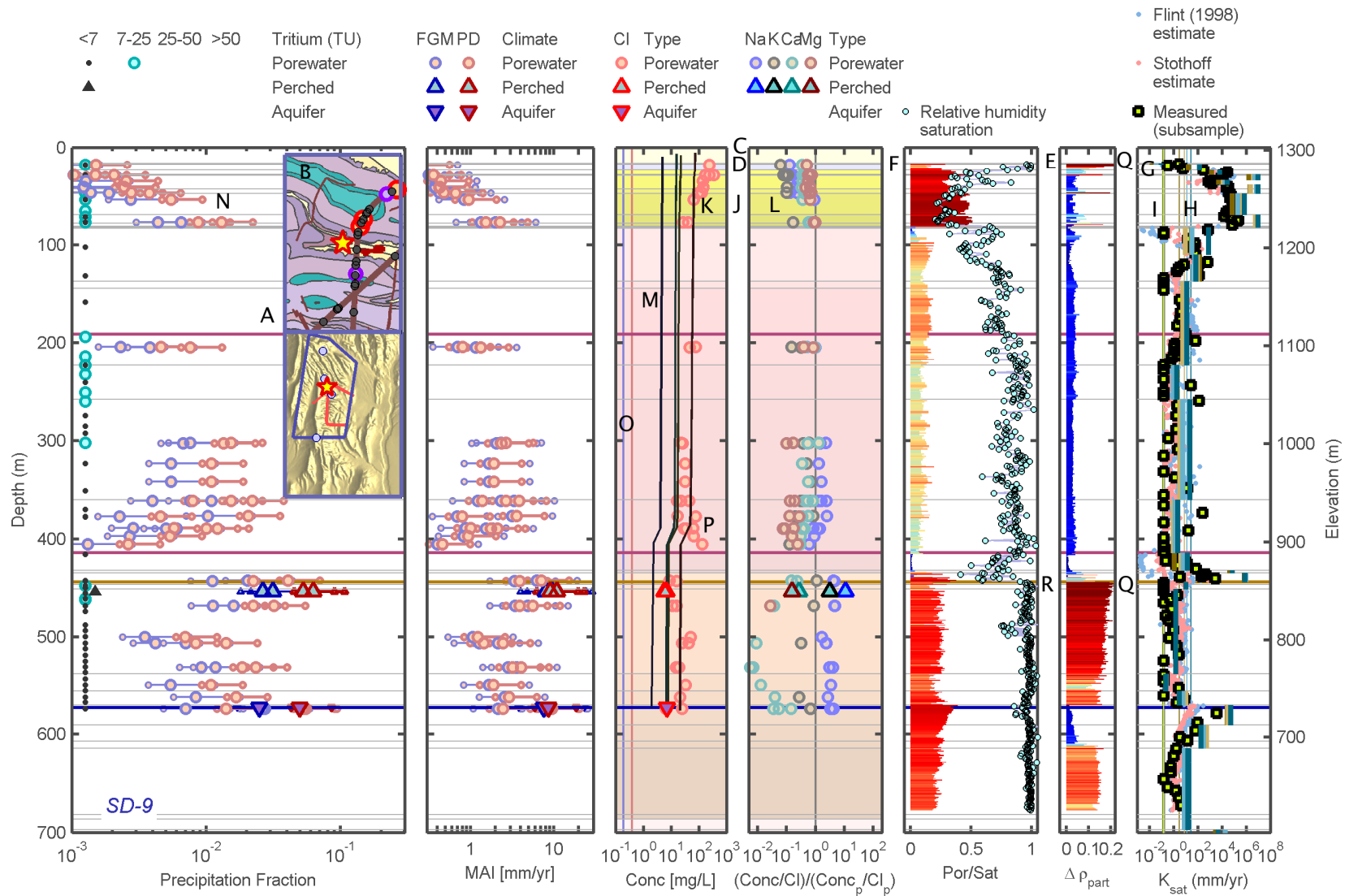


Figure 3-5. Geochemical Observations for SD-9 and Associated Thermohydrologic Properties. Chloride Profiles Digitized From Sandia National Laboratories (2007a, Figure 6.5-3). [1 m = 3.28 ft; 25.4 mm/yr = 1 in/yr; 1 mg/L = 1 ppm]

Figure 2-2, SD-9 is near the center of the potential repository footprint. The insets also indicate that SD-9 is located low on a ridge just above a wash bottom. Samples from several locations in the nearby ESF, under the upper parts of the hillslopes in the same wash, have an inferred or potential bomb-pulse signature.

The ridge north of SD-9 exposes an outcrop sequence of (from uppermost to lowermost) Tcr2, Tcr1, Tcpum, Tcpll, and Tcpln (referring to Figure 2-1 to link colors with units), with a possibly shallowly dipping fault mapped approximately 100 m [330 ft] updip (B in Figure 3-5). The Tcr2 and Tcr1 are part of the caprock sequence with relatively high ITYM-estimated MAI fluxes (Stothoff, 2008a). The Tcpll and the upper portion of the Tcpum are lithophysal zones; Stothoff (2008a) infers lithophysal zones as having relatively low potential MAI fluxes. The base of the Tcpum zone and the Tcpln zone are nonlithophysal zones; Stothoff (2008a) infers nonlithophysal zones as having MAI fluxes intermediate between the caprock and lithophysal zones. The vitric Tcpcv lies below the Tcpln and, where present, the Tcplnc zones. The GFM2000 model (Bechtel SAIC Company, LLC, 2004a) subdivides the Tcpcv into the three uppermost differentiated GFM2000 layers and combines all overlying layers into a single undifferentiated TCw tuff layer. The undifferentiated unit is indicated by a gray zone in the middle panels, but it cannot be distinguished in Figure 3-5, because it is only 1.1 m [3.6 ft] thick at this location. The GFM2000 model begins the PTn unit with the lowermost of its three distinct Tcpcv layers.

The rightmost panels provide clues regarding possible pathways of water through the system at SD-9. The pale yellow region at the top of the middle panels (C in Figure 3-5) indicates unconsolidated material, typically alluvium and colluvium but possibly also drill-pad fill. The unconsolidated cover is approximately 16 m [54 ft] at this location. Stothoff (2008a) found that 10 m [33 ft] of soil cover above bedrock provides protection from bare-soil evaporation in one-dimensional infiltration simulations, so this thickness of cover may allow water to collect for extended periods of time at the interface of low-permeability bedrock, slowly draining into the bedrock, unless plant roots are able to reach the moist layer. The borehole log for SD-9 does not distinguish between fill material used to construct the drill pad and the original soil profile. Most of the indicated soil thickness is likely drill-pad fill, based on observations at trenches in similar topographic locations that indicate soil thickness is limited to less than 3 m [10 ft] and the greatest observed thickness in the relatively well-preserved remnant terraces in Split Wash (at an analogous topographic position two wash systems to the south) is approximately 7 m [23 ft] (Stothoff, 2008b). In these shallower soils, evapotranspiration would tend to remove the water collected over a bedrock interface and net infiltration into the bedrock faces competition from evapotranspiration.

The Tcpcv zone, a layer of nearly saturated welded tuff at the base of the TCw unit indicated by the thin pale blue band (marked as D in Figure 3-5), lies under the unconsolidated cover. Near-saturation conditions are indicated by an E in Figure 3-5. The nearly saturated conditions are associated with porosity less than 0.2 (marked by an F in Figure 3-5) and saturated hydraulic conductivity (K_{sat}) approximately (to within an order of magnitude or two) the same magnitude (marked by a G in Figure 3-5) as inferred areal-average infiltration rates. Gravity drainage of water in the unsaturated zone typically imposes near-saturated conditions when percolation fluxes are greater than matrix K_{sat} , but can also impose near-saturated conditions when percolation fluxes are somewhat smaller than matrix K_{sat} . It is reasonable to infer that fracture and fault fluxes occur when matrix K_{sat} is much smaller than percolation fluxes and that fracture and fault fluxes are inhibited when matrix K_{sat} is much larger than percolation fluxes, but it is more difficult to draw firm conclusions when the two are of comparable magnitude.

Saturated hydraulic conductivity values Flint (1998) and Stothoff (2008a) estimated for core samples and Flint (1998) measured on core subsamples all have values between the 10th and 50th percentiles of areal-average MAI in the Sandia National Laboratories (2007a) three-dimensional unsaturated zone flow and transport model. The calibrated layerwise matrix K_{sat} values used in the Sandia National Laboratories (2007a) model are above the corresponding areal-average MAI for all four maps. Direct comparison of the K_{sat} values is complicated because the layerwise K_{sat} values represent a spatial scale many orders of magnitude larger than the core samples. The four thin vertical lines (marked by an H in Figure 3-5) indicate the 10th, 30th, 50th, and 90th percentiles of areal-average MAI, colored brown, tan, cyan, and blue in sequence. The sequences of thick vertical lines, mostly changing at layer boundaries, represent layerwise calibrated matrix K_{sat} values for the MAI map with the corresponding line color. Note that the olive vertical line (marked by an I in Figure 3-5) is the experimental limit for determining K_{sat} ; measurements on the olive line likely have smaller K_{sat} than the line.

The transition zone between the TCw and PTn units may be a relatively likely location for perching to occur under wetter climatic conditions because it has elevated saturation levels in various boreholes and is associated with damp spots observed during tunneling within the ESF, but flowing water has not been reported in the transition zone. Areas where the matrix is saturated are indicators that at least some of the fractures, where present, may also be carrying water. In areas where a low-permeability matrix is both saturated and relatively unfractured, inducing perching above the layer, lateral flow may become activated in the fracture system above the unfractured layer. Such lateral flow would tend to spread waters from high-infiltration areas into low-infiltration areas, with a superimposed trend toward the downdip direction, as the water moves into local breaches in the restrictive layer from faults, fractures, or other local heterogeneities. Because net infiltration in deep alluvium is generally small in low-precipitation areas such as Yucca Mountain (Stothoff and Walter, 2007), the water causing the wet conditions at this borehole may be due to episodic flooding or lateral flow from nearby areas with shallow soil thickness.

The yellow band below the thin TCw layer (marked by a J) indicates the nonwelded PTn unit. In SD-9, sampled chloride concentrations drop nearly monotonically across the thickness of the PTn, indicated by a K, and other geochemical tracers become enriched relative to chloride across the same interval (indicated by an L). Associated hydraulic indicators in the rightmost panels are consistent with matrix-dominated flow through the PTn in the SD-9 core, based on K_{sat} values much larger than inferred MAI and saturation values less than 0.5 through most of the PTn thickness.

The reduction in pore water chloride concentration across the PTn at SD-9 may be a result of climate change. Some chloride profiles in the arid southwest shift from relatively large concentrations near the ground surface to relatively dilute concentrations at depth. These are often explained as the result of plug flow in the unsaturated zone preserving the chloride record from a period of relatively dry conditions during the middle to late Holocene after a relatively wet period during the Pleistocene. The relatively dry conditions imply that the chloride flux may be larger, because local sources of wind-eroded salt are exposed to a greater extent, and imply that waters entering the ground undergo evapotranspiration to a greater extent, thereby further raising soil-water chloride concentrations. Such a change in climate results in a bulge of relatively concentrated waters moving down through the unsaturated zone, implying that the relatively dilute concentrations at the base of the PTn could partially represent waters infiltrated during a wetter prior climate.

The chloride profile in SD-9 may also be consistent with lateral mixing of waters. Water entering the bedrock in areas with relatively deep soil is expected to have undergone extensive evapotranspiration, resulting in concentrated pore waters. Water entering in areas with shallow soil or in active channels is likely more dilute. If these waters gradually mix with depth, a profile located in a low-MAI zone becomes gradually more dilute with depth. A two-member mixing hypothesis at SD-9 is supported by the consistent change of all major-ion indicators with depth, even indicators that would be expected to change in opposite ways due to precipitation (Ca) or leaching (Na). The hypothesized two sources do not appear to have completely mixed at the bottom of the profile, because the sample concentrations are more dilute than the overlying samples. The major-ion indicators are the ratio of the concentration in the sample to the concentration in 3 Springs and Kawich Peak precipitation (CRWMS M&O, 2003), normalized by the corresponding chloride ratio.

The chloride concentrations displayed in the third panel require interpretation to estimate percolation flux. The black lines (marked by an M) in the third panel are the result of numerical simulations of chloride transport that Sandia National Laboratories (2007a) performed using a three-dimensional site-scale flow and transport model with four different infiltration rates. Moving from right to left (concentrated to dilute), the lines represent calculated concentrations using the 10th, 30th, 50th, and 90th percentile infiltration maps (and their associated chloride deposition fluxes) for present-day climate. The chloride-transport profile lines in this and following figures were digitized from figures Sandia National Laboratories (2007a) presented.

Rearranged forms of the chloride-mass-balance relationship provided in Eq. (3-1) provide another pair of methods to interpret chloride profiles. The precipitation fraction displayed in the left panel is the fraction of precipitation that becomes percolation flux; the same quantity is called recharge fraction when applied to recharge and is useful for comparing different locations (Stothoff and Musgrove, 2006). The precipitation fraction is defined by

$$\frac{q_w}{P} = \frac{c_p}{c_w} \quad (3-2)$$

The effective chloride concentration in precipitation is needed to calculate the precipitation fraction. The CRWMS M&O (2003) assumptions of 0.3, 0.35, and 0.6 mg/L [0.3, 0.35, and 0.6 ppm] for present-day c_p are used to estimate lowest, representative, and highest chloride concentrations in the left panel, yielding the estimates in pink (marked by an N). The larger circles denote the representative value, which increases by an order of magnitude with depth into the PTn, ending at approximately 1 percent. An alternative estimate for glacial conditions is indicated in blue, using an estimate of full-glacial-maximum c_p that is half the present-day c_p , following Zhu, et al. (2003), with an additional uncertainty of 20 percent. The representative precipitation fraction is approximately 0.5 percent at the base of the PTn. The representative c_p values for present-day and full-glacial conditions are indicated by thin pink and blue lines in the third panel (marked O).

Stothoff and Musgrove (2006) extrapolated upland recharge estimates from hydrobasins in east-central Nevada, which suggest that hydrobasin-average recharge fractions for the present-day precipitation at Yucca Mountain are approximately 2 to 3 percent. These estimates are derived for a much larger scale than Yucca Mountain, and Stothoff and Musgrove (2006) found that recharge estimates reported in the literature vary widely even with similar level of precipitation. Applying the same upland relationships to the

full-glacial-maximum climate estimates of Stothoff and Walter (2007), with mean annual precipitation between 1.6 and 2 times present, yields a precipitation fraction between 5 and 12 percent and representative precipitation fraction (mean annual precipitation of 1.75 times present) between 6 and 9 percent. Based on these extrapolated relationships, the representative precipitation fraction at SD-9 is a factor of 2 to 3 lower than the extrapolated upland recharge approach would estimate for present-day conditions and a factor of 12 to 18 times lower than the approach would estimate for full-glacial conditions.

The second panel displays a direct estimate of deep percolation using the relationship

$$q_w = P \frac{c_p}{c_w} \quad (3-3)$$

The estimates in the second panel apply to the borehole collar elevation in the Stothoff and Walter (2007) Orbital-Cycle Climate for Yucca Mountain middle precipitation model, with an assumed uncertainty of 20 percent, yielding estimates of 139, 174, and 218 mm/yr [5.5, 6.9, and 8.6 in/yr] for low, representative, and high present-day mean annual precipitation. The pink and blue symbols represent present day and full-glacial estimates using the same c_p assumptions as the leftmost panel. These assumptions yield similar estimates of approximately 2 mm/yr [0.08 in/yr] for MAI under the two climatic conditions, compared to the estimates of approximately 4 and between 10 and 14 mm/yr [0.16; between 0.39 and 0.51 in/yr] using the representative present-day and full-glacial assumptions.

The pink band in the middle panels represents the densely welded TSw unit. Fracture intensities are relatively high throughout most of the TSw, so that the fracture system is sufficiently permeable to carry percolation fluxes exceeding precipitation without perching in most of the TSw. The hydrologic indicators suggest that fracture flow may be occurring through most of the lower portions of the TSw at SD-9, based on the relatively high saturations and the estimates for K_{sat} that are comparable to and less than the areal-average MAI estimates. Chloride concentrations are relatively similar to the concentration at the base of the PTn through most of the potential-repository host horizon indicated by the GFM2000 model (which is bracketed by purple lines in all of the panels). Elevated chloride concentrations (marked with a P) are found at the base of the host horizon, associated with a zone with especially low porosity values. It is difficult to obtain sample water from low-porosity rocks, and the measured chloride concentrations may include rock chloride released as the rocks were crushed to obtain the water samples. The dip in relative major-ion concentrations at the same location further suggests that the sampling process may have included rock chloride at the base of the host horizon.

The presence of a low-permeability zeolitic zone is generally associated with perching below the potential-repository host horizon. At borehole SD-9, the top of the altered zeolitic zone (the brown line running across all of the panels) is approximately 30 m [98 ft] below the top of the CHn unit (the peach-colored zone in the middle panels), but the zeolitic zone is not always at the same stratigraphic location and is missing in some of the southern areas. For example, the zeolitic zone is almost 80 m [260 ft] below the top of the CHn in SD-7 (Figure 3-6). The red lines marked with an A in Figure 3-6 indicate the final step of hydraulic-property calibration that Sandia National Laboratories (2007b) used for SD-9, locally adjusting layerwise properties to account for the observed perching.

The degree that matrix particles increase in density when the sample is dried in the oven at 105 °C [221 °F] appears to be associated with alteration, especially in the zeolitic zone. Particles that become denser under heating imply that the particles swelled by the addition of water, thereby tending to decrease the pore space available for flow and to close fractures. Both factors tend to reduce bulk permeability. Elevated values of this indicator are shades of red in the $\Delta\rho_{\text{part}}$ panel, as marked with a Q in Figure 3-5. Elevated values of the $\Delta\rho_{\text{part}}$ indicator in the zeolitic zone appear to indicate that the bulk K_{sat} , combining both the matrix and fracture systems, is comparable to or less than the percolation flux; thus they may indirectly indicate areas with low fracture intensity. Elevated matrix saturations are consistently associated with elevated values of the $\Delta\rho_{\text{part}}$ indicator at and below the base of the TSw unit (see the figures in Appendices A and B).

Typically, one or more thin bands with elevated values of the $\Delta\rho_{\text{part}}$ indicator are also found within the PTn (see the figures in Appendices A and B). Elevated matrix saturations are consistently found above the uppermost band, which is associated with the low-permeability transition between the TCw and PTn, but are rarely associated with lower bands in the PTn lying within high-permeability subunits. Flint (1998) indicated that these bands are indicative of clay in the matrix. Flint (1998) described the uppermost band as pervasive across the site and as containing up to 35 percent smectite, which can increase in volume after hydration up to 300 times the dehydrated mineral size. From a hydraulic standpoint, the upper alteration band may act like a relatively unfractured low-permeability zone where the alteration closes the fracture apertures and forms a capillary barrier with the underlying unit.

The lower alteration bands within the PTn do not appear to have the same hydraulic effect as the uppermost band. Typically, lower bands have two to four orders of magnitude larger matrix permeability than the upper band and matrix saturation between approximately 0.2 and 0.5 (compared to saturations greater than 0.9 in the upper band). If the formation of clay in the PTn bands required that the matrix remained relatively wet for extended durations, then the presence of alteration bands where the matrix is relatively dry today implies that different percolation patterns existed when the clay formed. Present-day climatic conditions induce lower percolation fluxes than under past glacial conditions, but formation of the thin low-permeability upper band may have changed the spatial distribution of percolation by promoting localized flow paths.

Perched water is suggested by the saturation levels that are approximately 1 (indicated with an R in Figure 3-5). Samples obtained from the perched water are indicated by upward-pointing triangles. Samples from the aquifer below the unsaturated zone are indicated by downward-pointing triangles, with the average static water level Bechtel SAIC Company, LLC (2004c) reported indicated by the blue line. The static water level Sass, et al. (1988) reported is indicated by the blue line in boreholes not described by Bechtel SAIC Company, LLC (2004c). The perched water samples have more dilute chloride concentrations than any of the matrix samples, although the matrix samples in the perched water zone are more dilute than the other matrix samples. CRWMS M&O (2003) indicates that perched and aquifer waters tend to have similar major ion geochemistry (as is the case for chloride in SD-9) but differ in isotopic characteristics, such as δ -13C, δ -87Sr, and U-234/U-238 activity ratios, not shown in the borehole figures. CRWMS M&O (2003) discusses the geochemistry of perched water in detail, including inferences related to residence time and sources of infiltrating water.

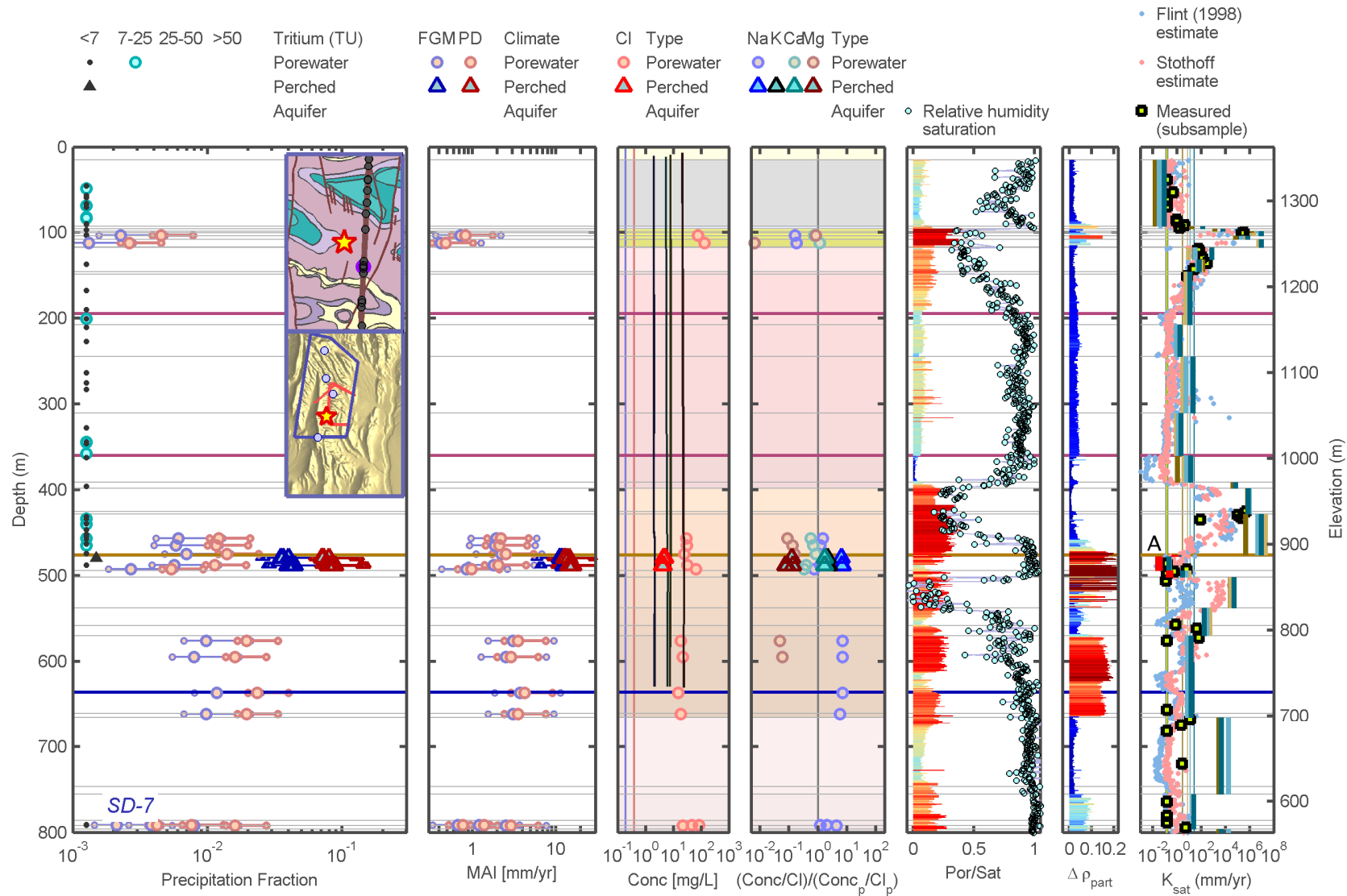


Figure 3-6. Geochemical Observations for SD-7 and Associated Thermohydrologic Properties. Chloride Profiles Digitized From Sandia National Laboratories (2007a, Figure 6.5-8). [1 m = 3.28 ft; 25.4 mm/yr = 1 in/yr; 1 mg/L = 1 ppm]

The perched water in SD-9 has dilute chloride concentrations relative to pore waters above and below the perched zone, which may be due to some combination of distinct matrix and fracture pathways contributing waters with dissimilar characteristics, dissimilar ages for matrix and perched waters, and lateral flow within the perched zone contributing waters with different shallow subsurface characteristics. Figures 3-7 through 3-9 show, from south to north, geochemical and hydrologic observations for boreholes UZ #16, SD-12, and NRG-7a. Perched water samples obtained from SD-7 and NRG-7a are more dilute than the pore waters at the same depths, in common with SD-9. MAI estimated at SD-7 using the representative present-day assumptions is approximately 12 to 16 mm/yr [0.47 to 0.63 in/yr] for the perched water and 1 to 2 mm/yr [0.04 to 0.08 in/yr] for matrix pore waters at the same elevation. At SD-9, corresponding concentrations are approximately 9 to 11 mm/yr [0.35 to 0.43 in/yr] and 4 to 7 mm/yr [0.16 to 0.28 in/yr], respectively, and at NRG-7a, corresponding concentrations are approximately 6 to 9 mm/yr [0.24 to 0.35 in/yr] and 1 to 2 mm/yr [0.04 to 0.08 in/yr], respectively. Note that the nonwelded PTn is less than 20 m [66 ft] thick at SD-7, whereas it is approximately 55 and 60 m [180 and 200 ft] thick at SD-9 and NRG-7a, respectively, consistent with the idea that perched waters and pore waters may be in closer chemical equilibrium below the PTn where the PTn is thicker. Also note that numerous faults are identified within and near the SD-7 borehole (located on Highway Ridge), and the top 15 m [50 ft] indicated as alluvium/colluvium in Figure 3-6 is actually pad fill material (Bechtel SAIC Company, LLC, 2006) that has only

recently begun to affect infiltration at SD-7. Like SD-7, pore water chloride in UZ-14 is approximately an order of magnitude more concentrated than perched water chloride (shown in Appendix A), but the PTn is approximately 64 m [210 ft] thick at UZ-14. The perched waters in UZ-14 have a chemical signature that may have been influenced by drilling fluids from borehole G-1 (CRWMS M&O, 2003); thus the geochemical disequilibrium suggested by the UZ-14 samples may not be representative of undisturbed conditions.

The left edge of the left most panel in each borehole figure has a series of tritium observations, characterized by the degree to which the waters have a bomb-pulse signature. The tritium color codes in the first panel represent premodern conditions; potential or partial indication of a bomb-pulse signature; a value in the low range of unambiguous bomb-pulse signature; and a value in the high range of unambiguous bomb-pulse signature. Based on these categories, borehole SD-9 has a potential or partial indication of bomb-pulse tritium interspersed with premodern samples through the unsaturated zone to the level of the perched water, but the perched water does not contain sufficient bomb-pulse tritium to be analytically detectable. Note that tritium is a hydrogen isotope, and hydrogen is one of the atoms of the water molecule; thus elevated tritium levels may indicate water movement as vapor instead of as liquid.

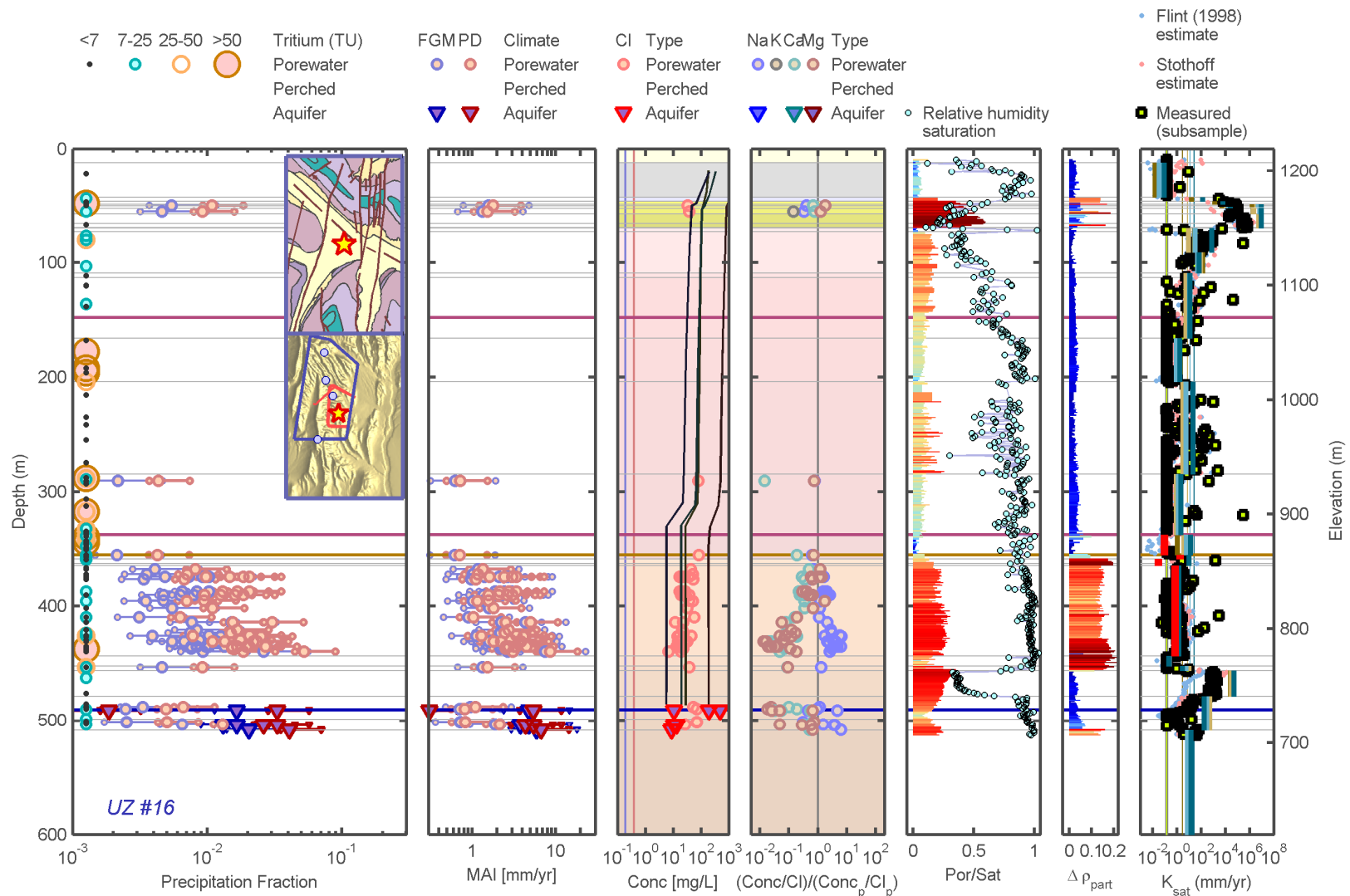


Figure 3-7. Geochemical Observations for UZ #16 and Associated Thermohydrologic Properties. Chloride Profiles Digitized From Sandia National Laboratories (2007a, Figure 6.5-11). [1 m = 3.28 ft; 25.4 mm/yr = 1 in/yr; 1 mg/L = 1 ppm]

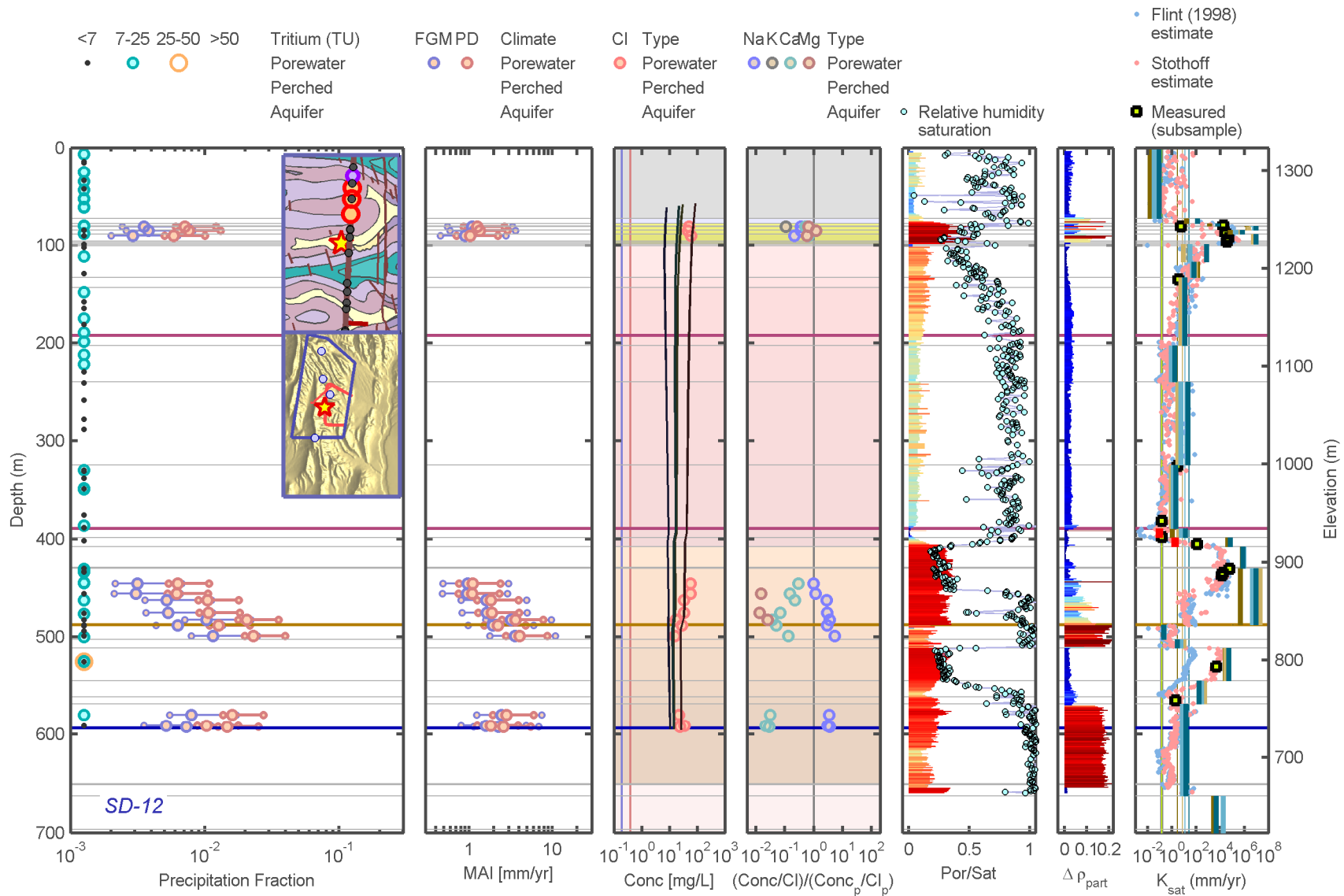


Figure 3-8. Geochemical Observations for SD-12 and Associated Thermohydrologic Properties. Chloride Profiles Digitized From Sandia National Laboratories (2007a, Figure 6.5-1). [1 m = 3.28 ft; 25.4 mm/yr = 1 in/yr; 1 mg/L = 1 ppm]

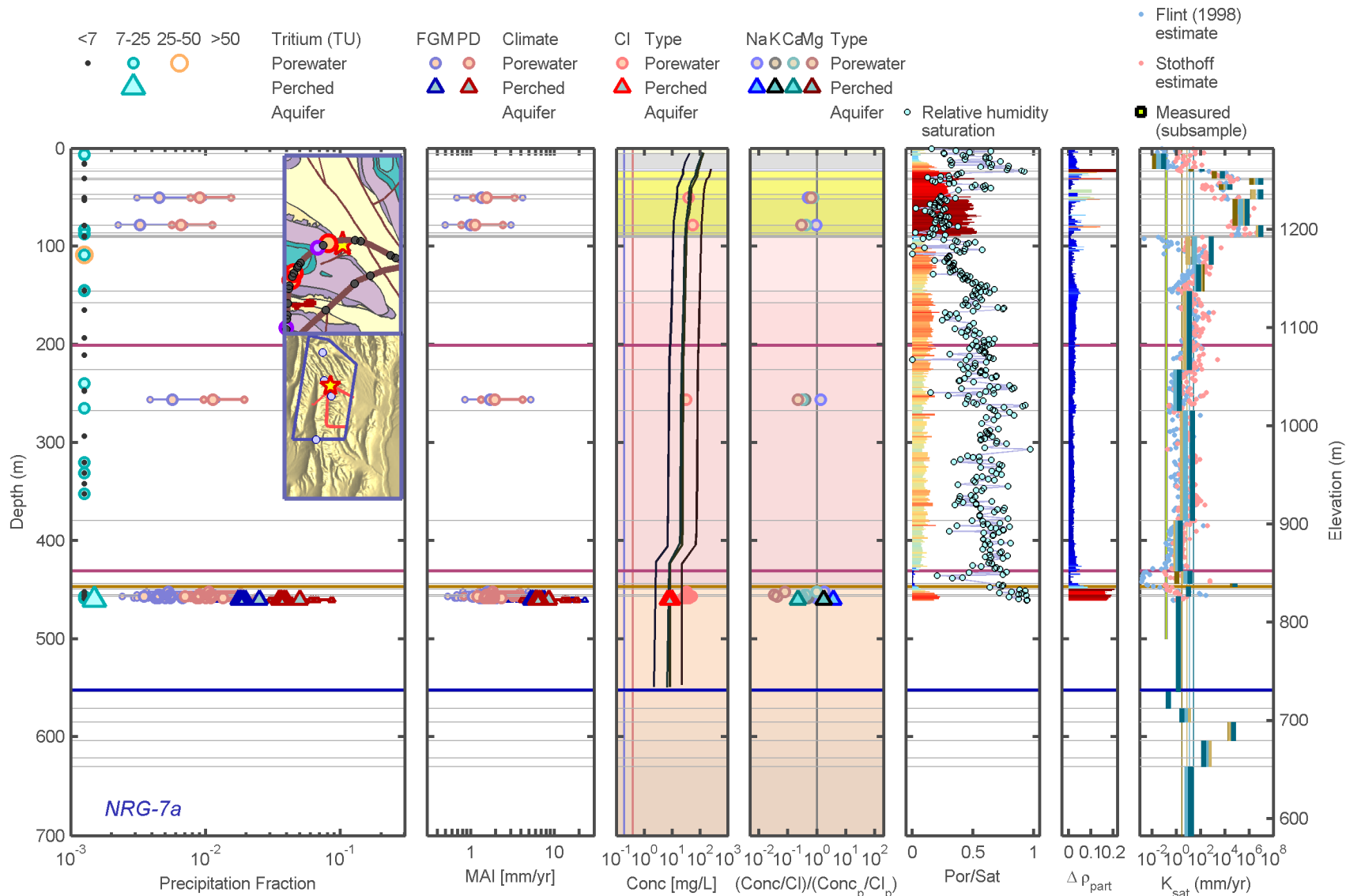


Figure 3-9. Geochemical Observations for NRG-7a and Associated Thermohydrologic Properties. Chloride Profiles Digitized From Sandia National Laboratories (2007a, Figure 6.5-7). [1 m = 3.28 ft; 25.4 mm/yr = 1 in/yr; 1 mg/L = 1 ppm]